

# A Monte Carlo Tree Search Framework for Quantum Circuit Transformation

Xiangzhen Zhou<sup>1,2</sup>, Yuan Feng<sup>\*1</sup> and Sanjiang Li<sup>†1</sup>

<sup>1</sup>Centre for Quantum Software and Information, Faculty of Engineering and Information Technology, University of Technology Sydney, NSW 2007, Australia

<sup>2</sup>State Key Lab of Millimeter Waves, Southeast University, Nanjing 211189, China

April 26, 2022

## Abstract

In Noisy Intermediate-Scale Quantum (NISQ) era, quantum processing units (QPUs) suffer from, among others, highly limited connectivity between physical qubits. To make a quantum circuit executable, a circuit transformation process is necessary to transform it into a functionally equivalent one so that the connectivity constraints imposed by the QPU are satisfied. While several algorithms have been proposed for this goal, the overhead costs are often very high, which degenerates the fidelity of the obtained circuits sharply. One major reason for this lies in that, due to the high branching factor and vast search space, almost all these algorithms only search very *shallowly* and thus, very often, only (at most) locally optimal solutions can be reached. In this paper, we propose a Monte Carlo Tree Search (MCTS) framework to tackle the circuit transformation problem, which enables the search process to go much deeper. The general framework supports implementations aiming to reduce either the size or depth of the output circuit through introducing SWAP or remote CNOT gates. The algorithms, called MCTS-Size and MCTS-Depth, are polynomial in all relevant parameters. Empirical results on extensive realistic circuits and IBM Q Tokyo show that the MCTS-based algorithms can reduce the size (depth, resp.) overhead by, on average, 66% (84%, resp.) when compared with t|ket>, an industrial level compiler.

## 1 Introduction

With Google’s recent conspicuous, though arguable, success in demonstrating quantum supremacy in a 53-qubit quantum processor [1], NISQ (Noisy Intermediate-Scale Quantum) devices have attracted rapidly increasing interests from researchers in both academic and industrial communities. *Quantum processing units* (QPUs) in the NISQ era only support a limited set of basic operations (elementary quantum gates) and often suffer from high gate errors, short coherence time, and limited connectivity between physical qubits. In order to run a quantum algorithm, described as a quantum circuit, we need to *compile* the circuit (referred to as *logical circuit* henceforth) into a functionally equivalent *physical circuit* executable on the QPU. The compilation includes two basic processes. In the *decomposition* process, gates in the logical circuit are decomposed, or transformed, into elementary gates supported by the QPU [2, 3, 4]. The *transformation* process, initiated in [5, 6] and also known as *quantum circuit transformation* (QCT) [7] or *qubit mapping* [8], is then performed on the generated circuit, which further consists of two steps: *initial mapping construction* and *qubit routing*. The former process constructs a mapping that maps qubits in a logical circuit, called *logical qubits*, to the ones in the QPU, called *physical qubits*; while the latter transforms a circuit through adding ancillary operations like SWAP gates to ‘route’ physical qubits in order to make all multi-qubits gates executable.

---

<sup>\*</sup>yuan.feng@uts.edu.au

<sup>†</sup>sanjiang.li@uts.edu.au

Both the decomposition and the transformation processes have been studied extensively in the literature. As there are now standard decomposition processes (see, e.g., [9, Chapter 4]), in this paper, we focus on the transformation process, and assume that gates in the input logical circuit have been well decomposed into elementary gates that are supported by the QPU. Furthermore, we assume that an initial mapping is given, which can be obtained by employing, say, the greedy strategy [10, 11, 12], the reverse traversal technique [8], the simulated annealing based algorithm [13], or the subgraph isomorphism based methods [5, 14, 15].

To reduce the gate overheads in the qubit routing step, many algorithms have been proposed aiming at minimising gate counts [10, 13, 15, 16], circuit depths [17, 18, 19, 20] or circuit error [21, 22]. These algorithms can be roughly classified into two broad categories (see also [23] for a similar classification). The first category consists of algorithms that try to reformulate QCT as a planning or optimisation problem and solve it by applying off-the-shelf tools [19, 20, 24, 25, 26, 22, 27, 28]. However, as shown in [24, 7], QCT is NP-complete in general. Algorithms in this category are usually highly unscalable when the size of input circuits becomes large.

In contrast, algorithms in the second category use heuristic search to construct the output quantum circuit step by step from the original input quantum circuit [8, 11, 10, 24, 29, 30, 13]. Experimental results show that customised heuristic search algorithms are more promising in transforming large-scale circuits, but usually there is still a considerable gap between the output circuit and an optimal one. The reason partially lies in the limited search depth in most of these algorithms. To achieve efficiency, one either divides the circuits into layers and tries to execute the gates layer-wise [10], or simply considers only the direct effect of a single move (i.e., SWAP) (see e.g., [8, 7, 12]). This leads to a very shallow search depth. The Simulated Annealing and Heuristic Search algorithm (SAHS) [13] and the Filtered and Depth-Limited Search approach (FiDLS) [15] can go one or two steps further, but exploring even more seems impractical as the searching process will become very slow if many qubit connections are present in the QPU.

Inspired by the recent spectacular success of Monte Carlo Tree Search (MCTS) in Computer Go play [31, 32], in this paper, we propose an MCTS framework for the QCT problem. Although first designed for solving computer games, MCTS has found applications in many domains which can be represented as trees of sequential decisions [33]. MCTS is a flexible statistical anytime algorithm, which can be used with little or no domain knowledge [33]. The basic idea behind MCTS is to explore and exploit, in a balanced way, a search tree in which each node represents a game state and each branch a legal move starting from that state. Given the current game state, the aim is to select the most promising move by exploring a search tree rooted with this state, based on random sampling of the search space. This is achieved through the following five steps: (1) *Selection*. Starting from the root, we first select successively a child node until a leaf node is reached; (2) *Expansion*. Expand the selected leaf node with one or more child nodes each of which corresponding to a legal move; (3) *Simulation*. Play out the task to completion by selecting subsequent moves randomly; (4) *Backpropagation*. Backpropagate the simulation result (winning, losing, or the reward points collected) towards the root node to update the values of nodes along the way; (5) *Decision*. After repeated a sufficient number of times, we then select the best move (with the largest value) and move to the next game state.

**Example 1.** We show how to conduct a full playout based on a search tree as shown in Fig. 1(a). Suppose a simple strategy only choosing child with maximum winning rate<sup>1</sup> is used in Selection. Then starting from root node 0, nodes 2 and 6 with maximum  $\#wins/\#simulations$  values 4/6 and 2/2 among their peers according to the data in column ‘EBBP’, Evaluation Before BackPropagation, in Fig. 1(c) will be chosen successively. Because node 6 is a leaf, it will be expanded and its child nodes 8 and 9, as shown in the dashed box of Fig. 1(b), will be opened. After Expansion, one or more newly opened nodes will be chosen to perform simulations. In this example, both nodes 8 and 9 are chosen to execute 2 random simulations and the results are assumed to be 0/2 and 1/2 respectively. After all simulations in node 8 are done, the result will be back propagated to root node 0 through nodes 6 and 2, and their values will be updated and are marked red in the ‘EABP1’, Evaluation After BackPropagation, column of Fig. 1(c). To be specific, the denominator values of nodes 6, 2 and 0 along the backpropagation path will be increased by 2 because the same number of new simulations are done in node 8; only the numerator values of white nodes 6 and 0 are increased because the black player lost both simulations. The same operation applies after the simulations in node 9 are finished and the updated values can be found in the ‘EABP2’ column.

<sup>1</sup>The strategy for *Selection* in practice is much more complex than this and should take both evaluations and time of visits into account. Interested readers can refer to [34, 35] for further details.

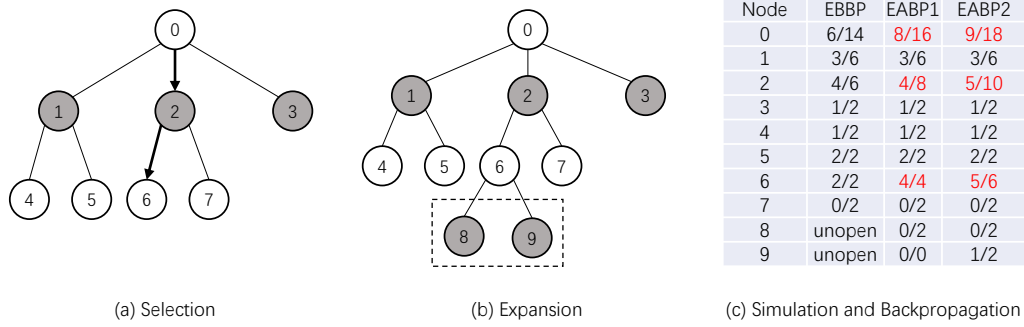


Figure 1: Example for one playout in MCTS. Each grey or white node in (a) and (b) represents a legal move made by the corresponding player. The last three columns in (c) represent, respectively, evaluations in each node before, after the first, and after the second *Backpropagation*. The evaluation is defined as  $\#wins/\#simulations$  obtained by *Simulation* and *Backpropagation*.

Our MCTS framework for the QCT problem also consists of these five major modules. In the framework, we adopt a fast random strategy for simulation and carefully design a scoring mechanism which takes both short and long-term rewards into consideration. Based on the five modules and the scoring mechanism, an algorithm, abbreviated as MCTS-Size, is proposed to optimise the size of the output circuit. The algorithm is polynomial in all relevant parameters and experiments on an extensive set of realistic benchmark circuits show that the search depth can easily exceed most, if not all, existing algorithms. The search depth in the proposed algorithm is defined as the depth of the selected leaf node to the root during each invoking of the Selection module. In Example 1, node 6 is chosen in Selection and its search depth is 2. This deep search method can reduce the gate overhead of the output physical circuits by a large margin when compared with the state-of-the-art algorithms [13, 15, 12] on IBM Q20.

Although aiming to optimise the circuit size in terms of gate numbers, MCTS-Size also reduces the depth of the output circuit significantly. Depth is also a significant criteria for quantum circuits due to the highly limited coherence time in NISQ devices. When compared with  $t|ket\rangle$  introduced in [12], a state-of-the-art and industrial level algorithm aiming at depth optimisation, MCTS-Size reduces the circuit size and depth overheads by, respectively, 66% and 75% on IBM Q20 (cf. Table 1). More importantly, as our MCTS framework is flexible, it can be easily adapted to accommodate various optimisation criteria. To exemplify this feature, we design MCTS-Depth by introducing two very simple modifications to MCTS-Size. Experimental results on IBM Q20 show that, compared to  $t|ket\rangle$  again, MCTS-Depth is able to reduce the depth overhead up to 84%.

This paper is a significant extension of the conference paper [36] presented at ICCAD’20. Among others, we have made the following major extensions: (a) aiming to optimise the output circuit depth, we design the MCTS-Depth algorithm (cf. Sec. 4) (note that [36] only considered optimisation of the output circuit size); (b) to further demonstrate the flexibility of our framework, we incorporate remote CNOT gates into the MCTS-based algorithms (cf. Sec. 5); (c) we describe in detail the parameter selection process and empirically compare the search depth of the MCTS-Size algorithm with that of SAHS [13] (cf. Sec. 6); and (d) we present detailed and additional empirical evaluation results (considering depth reduction as well as the effect of remote CNOT gates) on both IBM Q20 and a hypothetical grid-like QPU, called Grid  $5 \times 4$ , which also has 20 qubits but fewer edge connections than IBM Q20 (cf. Sec. 6).

The remainder of this paper is organised as follows: Sec. 2 provides some background knowledge about quantum computation and summarises the state-of-the-art of the quantum circuit transformation problem. Sec. 3 then presents a detailed description of the MCTS framework as well as a theoretical analysis. The adapted depth-optimisation algorithm is presented in Sec. 4. After that, we show how to incorporate remote CNOT in the MCTS-based algorithms in Sec. 5. Empirical evaluations of both MCTS-based algorithms on an extensive set of realistic benchmark circuits and on both IBM Q20 and Grid  $5 \times 4$  are presented in Sec. 6. The last section concludes the paper with an outlook.

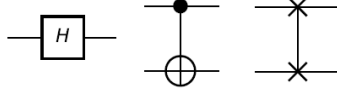


Figure 2: Hadamard, CNOT and SWAP gates (from left to right).

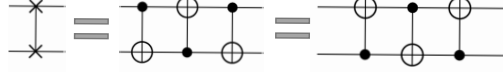


Figure 3: The decomposition of a SWAP into three CNOT gates.

## 2 Quantum Circuit Transformation

In classical computing, data are stored in the form of bits which have two states, 0 and 1. In contrast, data in quantum computing are stored in *qubits*, which also have two basis states represented by  $|0\rangle$  and  $|1\rangle$ , respectively. However, unlike a classical bit, a qubit can be in the superposition  $\alpha|0\rangle + \beta|1\rangle$  of basis states, where  $\alpha$  and  $\beta$  are complex numbers satisfying  $|\alpha|^2 + |\beta|^2 = 1$ .

The state of a qubit can be changed by quantum gates, which are mathematically represented by unitary matrices. Fig. 2 depicts three important quantum gates used in this paper: Hadamard, CNOT and SWAP gates. Hadamard is a single-qubit gate that has the ability to generate superposition: it maps  $|0\rangle$  to  $(|0\rangle + |1\rangle)/\sqrt{2}$  and  $|1\rangle$  to  $(|0\rangle - |1\rangle)/\sqrt{2}$ . CNOT and SWAP are both two-qubit gates. CNOT flips the target qubit depending on the state of the control qubit; that is, CNOT:  $|c\rangle|t\rangle \rightarrow |c\rangle|c \oplus t\rangle$ , where  $c, t \in \{0, 1\}$  and  $\oplus$  denotes exclusive-or. SWAP exchanges the states of its operand qubits: it maps  $|a\rangle|b\rangle$  to  $|b\rangle|a\rangle$  for all  $a, b \in \{0, 1\}$ . Note that a SWAP gate can be decomposed into three CNOT gates as shown in Fig. 3.

Quantum gates can be concatenated to form complex *circuits* which, together with measurements, are used to describe quantum algorithms. A circuit is usually denoted by a pair  $(Q, C)$ , where  $Q$  is a set of qubits and  $C$  a sequence of quantum gates on  $Q$ . Sometimes we also call  $C$  a circuit when  $Q$  is clear from the context. Fig. 4 shows a circuit where  $Q = \{q_0, \dots, q_4\}$ ,  $C = (g_0, \dots, g_4)$ ,  $g_0 = \text{CNOT}(q_0, q_2)$ ,  $g_1 = \text{CNOT}(q_3, q_4)$ , etc. Here each CNOT is annotated with the qubits on which they are applied.

### 2.1 Quantum Circuit Transformation

As mentioned in the introduction, to run a quantum circuit on a given QPU in the NISQ era, we need to transform it so that the connectivity constraints imposed by the QPU are all satisfied. Such connectivity constraints are typically described as an undirected and connected graph  $AG = (V, E)$ , called the *architecture graph* [7], where  $V$  denotes the set of physical qubits of the QPU and  $E$  the pairs of physical qubits on which a two-qubit gate can be applied.

Note that by a standard process [9], any quantum circuit can be decomposed into a functionally equivalent one which consists of only CNOT and single-qubit gates. Furthermore, as single-qubit gates can be executed directly on a QPU (connectivity constraints only prevent two-qubit gates from applying on certain pairs of physical qubits), if not otherwise stated, we assume that single-qubit gates have been removed and the circuit to be transformed consists solely of CNOT gates.<sup>2</sup> Note that this is only a technical assumption and, whenever necessary, we can always add back the corresponding single-qubit gates (cf. Sec. 4). Besides that, the SWAP gates added during the transformation process will be decomposed into CNOTs in the end.

An important notion related to quantum circuits which plays a key role in QCT is the *dependency graph*. Let  $C = (g_0, g_1, \dots)$  be a quantum circuit. We say gate  $g_i$  in  $C$  *depends* on  $g_j$  if  $j < i$  and they share at least one common qubit. The dependence is *direct* if there is no gate  $g_k$  with  $j < k < i$  such that  $g_i$  depends on  $g_k$  and  $g_k$  depends on  $g_j$ . In general, we can construct a directed acyclic graph (DAG), called the dependency graph [37], to characterise the dependency between gates in a circuit. Specifically, each node of the dependency graph

<sup>2</sup>This implies that we cannot simplify the circuits by, say, cancelling two consecutive CNOT gates acting on the same pair of qubits.

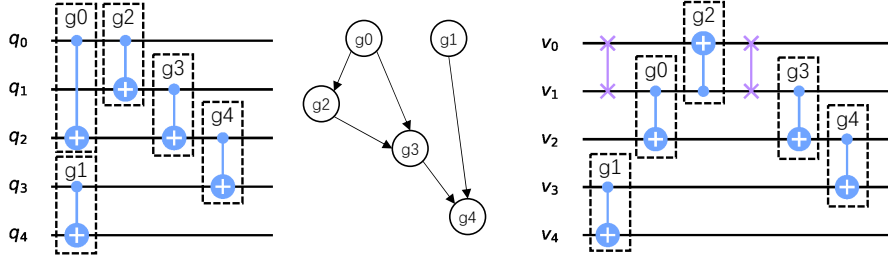


Figure 4: A quantum circuit (left), its dependency graph (middle) and the circuit after transformation (right).

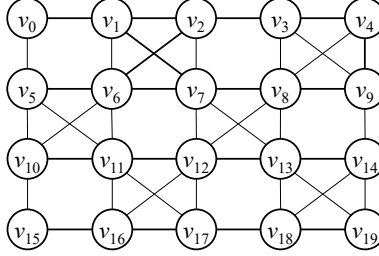


Figure 5: The architecture graph for IBM Q20.

represents a gate and each directed edge the direct dependency relationship between the gates involved. Let's say a gate  $g_i$  directly depends on  $g_j$ , then the corresponding edge  $(g_j, g_i)$  should be added to the dependency graph. With the help of dependency graph, any quantum circuit  $C$  can be divided into different *layers* such that gates in the same layer can be executed in parallel. The first or front layer, denoted by  $\mathcal{L}_0(C)$ , consists of the gates which have no parents in the DAG. The second layer,  $\mathcal{L}_1(C)$ , is then the front layer of the DAG obtained by deleting all gates in  $\mathcal{L}_0(C)$ . Analogously, we can define the  $i$ -th layer of a circuit for any  $i \geq 0$ .

**Example 2.** Fig. 4 shows an example of a quantum circuit (left) and its dependency graph (right), from which we can see that the front layer of the circuit consists of  $g_0$  and  $g_1$ , the second  $g_2$ , the third  $g_3$ , and the fourth  $g_4$ .

Another key notion for QCT is a qubit mapping  $\tau$  which allocates logical qubits  $Q$  to physical qubits  $V$  so that for any  $q_i, q_j \in Q$ ,  $\tau(q_i) = \tau(q_j)$  if and only if  $i = j$ . Given a logical circuit  $(Q, C)$  and an architecture graph  $AG$ , a two-qubit gate  $g = \text{CNOT}(q_i, q_j)$  in  $C$  is called *executable* by  $\tau$  if  $\tau(q_i)$  and  $\tau(q_j)$  are adjacent in  $AG$ , and  $g$  is either in the front layer of  $C$  or all the gates it depends on are executable. Note that in general it is impossible that all two-qubit gates in a circuit are executable by a single mapping. Once no gates are executable by the current mapping  $\tau$ , a QCT algorithm seeks to insert into the circuit some ancillary SWAP gates to change  $\tau$  into a new one so that more gates are executable. This insertion-execution process is iterated until all gates from the input circuits are executed. To illustrate the basic ideas, we revisit the circuit on the left side of Fig. 4.

**Example 3.** We transform the logical circuit  $LC = (Q, C^l)$  shown in Fig. 4 into a physical one  $PC = (V, C^p)$  satisfying the architecture graph  $AG$  in Fig. 5. Suppose the initial qubit mapping  $\tau$  is given as a naive one which maps  $q_i$  to  $v_i$ ,  $0 \leq i \leq 4$ .

1. Since  $\tau(q_3) = v_3$ ,  $\tau(q_4) = v_4$ , and  $v_3$  and  $v_4$  are adjacent in  $AG$ , gate  $g_1$  in  $C^l$  is already executable by  $\tau$ . Thus we initialise  $PC$  as a physical circuit with  $V = \{v_0, \dots, v_{19}\}$  containing only a single  $\text{CNOT}$  gate acting on  $v_3$  and  $v_4$ , and delete  $g_1$  from  $C^l$ . Thus now,  $C^l = (g_0, g_2, g_3, g_4)$  and  $C^p = (\text{CNOT}(v_3, v_4))$ .
2. As no gates in  $C^l$  is executable by  $\tau$ , we have to insert a SWAP (or a sequence of them) to get a new mapping which admits more  $\text{CNOT}$  gates from  $C^l$  executable. In this example, we choose to add  $\text{SWAP}(v_0, v_1)$  to  $C^p$ , which in effect converts  $\tau$  into  $\tau'$  that maps  $q_0$  to  $v_1$  and  $q_1$  to  $v_0$ . Now  $g_0$ , which

acts on  $q_0$  and  $q_2$ , is executable (since  $v_1$  and  $v_2$  are adjacent in  $AG$ ). Similarly,  $g_2$  is executable as well. Thus they can be deleted from  $C^l$  and added into  $C^p$  (with the operand qubits changed accordingly). Consequently, now  $C^l = (g_3, g_4)$  and

$$C^p = (CNOT(v_3, v_4), SWAP(v_0, v_1), CNOT(v_1, v_2), \\ CNOT(v_1, v_0)).$$

3. Proceeding in a similar way, we add another  $SWAP(v_0, v_1)$  to  $C^p$  to convert  $\tau'$  back to  $\tau$  so that  $g_3$  and  $g_4$  are executable. After deleting them from  $C^l$  and adding them into  $C^p$ , we have  $C^l = \emptyset$  and the final physical circuit becomes

$$C^p = (CNOT(v_3, v_4), SWAP(v_0, v_1), CNOT(v_1, v_2), \\ CNOT(v_1, v_0), SWAP(v_0, v_1), CNOT(v_1, v_2), \\ CNOT(v_2, v_3)),$$

which satisfies all the connectivity constraints of  $AG$ . The final physical circuit is shown in Fig. 4 (right).

## 2.2 Heuristic Search Algorithms

Recall that given a logical circuit  $LC_0$ , an architecture graph  $AG$ , and an initial qubit mapping  $\tau_{ini}$ , a QCT process aims to output a physical circuit which respects all the connectivity constraints in  $AG$ . To present this process as a search problem, we need to first define the notion of states. Naturally, a *state* of the QCT process is a triple  $\mathbf{s} = (\tau, PC, LC)$ , where  $\tau$  is a qubit mapping describing the current allocation of logical qubits,  $PC$  is the physical circuit that consists of all gates that have been executed so far and the auxiliary SWAP gates inserted, and the logical circuit  $LC$  consists of the remaining gates to be executed. Sometimes we denote by  $LC(\mathbf{s})$  and  $PC(\mathbf{s})$  the logical and the physical circuits of  $\mathbf{s}$ , respectively.

A *legal action* in the QCT process can be either a SWAP operation (corresponding to an edge in  $AG$ ) or a sequence of SWAP operations.<sup>3</sup> Let  $\mathbf{s} = (\tau, PC, LC)$  be the current state, and suppose an action  $SWAP(v_i, v_j)$  is taken on  $\mathbf{s}$ . Then a new state  $\mathbf{s}' = (\tau', PC', LC')$  is reached where  $\tau'$  is the same as  $\tau$  except that it maps  $\tau^{-1}(v_i)$  to  $v_j$  and  $\tau^{-1}(v_j)$  to  $v_i$ , where  $\tau^{-1}(v_i)$  and  $\tau^{-1}(v_j)$  are, respectively, the preimages of  $v_i$  and  $v_j$  under  $\tau$ . Furthermore,  $LC'$  is obtained from  $LC$  by deleting all gates which are executable by  $\tau'$ , and  $PC'$  is obtained from  $PC$  by adding first  $SWAP(v_i, v_j)$  and then all the gates just deleted from  $LC$ , with the operand qubits changed according to  $\tau'$ . While most algorithms select one SWAP each time, the  $A^*$  algorithm [10] and FiDLS [15] select a sequence of SWAPs. Note that when regarding sequences of SWAPs as legal actions, usually we execute a gate only after the last SWAP is applied.

Finally, the *initial state*  $\mathbf{s}_0$  of the QCT process is taken as  $(\tau_{ini}, PC_0, LC'_0)$  where  $PC_0$  is the physical circuit consisting of all gates from  $LC_0$  which are executable by  $\tau_{ini}$ , and  $LC'_0$  the logic circuit obtained by deleting all gates in  $PC_0$  from  $LC_0$ . The *goal states* are those with the associated logical circuit being empty. Note that the associated physical circuit of any goal state respects the connectivity restraints in  $AG$ . The *cost* of a state  $\mathbf{s}$  depends on the optimisation objective. In this paper, it can be either the total number of auxiliary gates inserted or the depth overhead of the stored physical circuit of  $\mathbf{s}$ . The aim of QCT is to find a goal state with the minimal cost w.r.t. the particular objective.

Many QCT algorithms in the literature adopt a divide-and-conquer approach in the search process. Starting from the current state  $\mathbf{s} = (\tau, PC, LC)$ , each subtask consists of executing the front layer, the first two layers, or a front section of the circuit. For example, in the  $A^*$  algorithm, a shortest path in  $AG$  (which corresponds to a sequence of SWAPs) is found which converts  $\tau$  to a new mapping so that all gates in the first two layers of  $LC$  are executable. In [12], Cowtan et al. partition  $LC$  into layers and then select the SWAP which can maximally reduce the diameter of the subgraph composed of all pairs of qubits in the current layer. Siraichi et al. [38] decompose  $LC$  into sub-circuits each of which leads to an isomorphic subgraph of  $AG$  and thus the corresponding embedding can act as a mapping  $\tau'$  that executes all gates in the sub-circuit. Their algorithm then tries to find a minimal sequence of SWAPs which converts  $\tau$  to  $\tau'$ . A similar approach is also adopted in Childs et al. [7].

<sup>3</sup>In Sec. 5 we will relax this restriction and allow remote CNOTs to be legal actions.

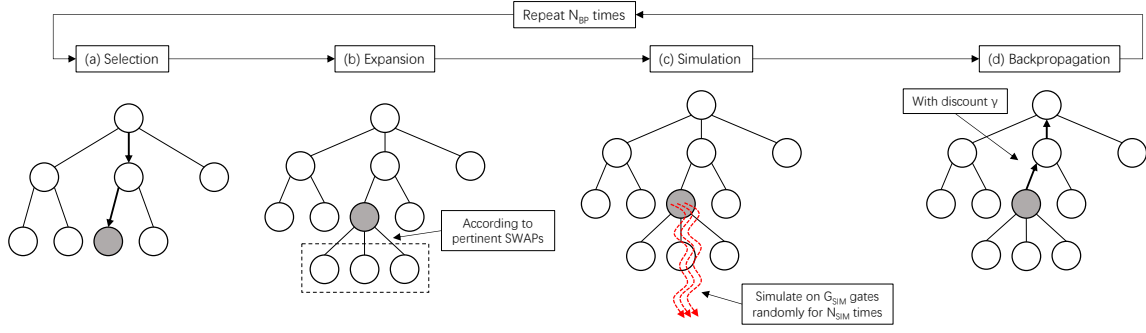


Figure 6: Overview of the Monte Carlo Tree Search Framework.

Unlike the above algorithms, SAHS [13] and FiDLS [15] do not divide the problem into sub-problems. Whenever a mapping is generated, they try to execute as many as possible gates from the logical circuit, no matter which level they are in. SAHS regards each SWAP as a valid action, but when selecting the best SWAP to enforce, it simulates the search process one step further and select the SWAP which has the best consecutive SWAP to apply. In principle, SAHS can go deeper but this will make the algorithm much slower (cf. Fig. 12 for an example). FiDLS regards any sequence with up to  $k$  SWAPs as a legal action and selects the sequence which executes the most number of gates per SWAP. In a sense, this means that its search depth can reach  $k$ . To ensure the running time is acceptable, in the experiments on Q20, FiDLS chooses  $k$  as 3 and introduces various filters to filter out unlike SWAPs.

### 3 The Proposed MCTS Framework

In this section, we describe an MCTS framework for quantum circuit transformation and present a detailed algorithm implementation. The algorithm, called MCTS-Size, aims at finding a goal state which has the minimal number of SWAPs inserted. Shortly in Sec. 4 we shall see this can be easily adapted to address other optimisation objectives.

Like general MCTS algorithms, our framework also consists of five major parts: *Selection*, *Expansion*, *Simulation*, *Backpropagation* and *Decision*. However, some significant modifications have been made to cater to the unique characteristics of QCT.

The Monte Carlo search tree for QCT, which is initialised immediately after the algorithm starts, stores all states having been explored during the transformation process. As stated in the previous section, an edge  $(s', s)$  connecting node  $s'$  and its child  $s$  indicates that a SWAP is applied to convert  $s'$  to  $s$ . With the aim to minimise the number of inserted gates, we define an immediate, short-term *reward* for each edge and a long-term *value* for each node of the search tree as follows.

**The short-term reward**  $\text{REW}(s', s)$  is the reward collected from the parent node  $s'$  to the child  $s$ , in terms of the number of gates executed by the newly inserted SWAP when this transition is made:

$$\text{REW}(s', s) = \# \text{gates\_in\_} LC(s') - \# \text{gates\_in\_} LC(s). \quad (1)$$

**The long-term value**  $\text{VAL}(s)$ . To determine the value of a state  $s$ , the following two factors are taken into account: (i) the number of inserted SWAPs when transformation of the remaining logical circuit is simulated at  $s$ . For efficiency, the simulation is performed on, instead of  $LC(s)$  itself, a fixed-sized sub-circuit of  $LC(s)$ . It is expected that the larger the sub-circuit is for simulation, the better simulated value will be obtained. (ii) the (simulated) value of its best child node and the reward to it collected from  $s$ . To be specific,

$$\text{VAL}(s) = \max\{\text{SIM}, \gamma \cdot [\text{REW}(s, s'') + \text{VAL}(s'')]\},$$

where  $\text{SIM}$  is the simulated value obtained from (i),  $s''$  is the child of  $s$  with the maximal value, and  $\gamma$  is a predefined discount factor satisfying  $\gamma < 1$ . In our later implementation,  $\text{VAL}(s)$  is initially assigned  $\text{SIM}$

in the *Simulation* module, and then updated in *Backpropagation*, whenever simulations are performed at a descendant of  $\mathbf{s}$ . Intuitively,  $\text{VAL}(\mathbf{s})$  describes the efficiency of introducing SWAPs (in terms of the average number of executed gates per SWAP) from  $\mathbf{s}$ , considering both the simulation at itself and the backpropagated one from this child nodes. Obviously, the larger  $\text{VAL}(\mathbf{s})$  is, the smaller the number of SWAPs needed to lead  $\mathbf{s}$  to a goal node, and the ‘better’  $\mathbf{s}$  is (compared with its siblings).

In addition to the above definitions, as shown in Fig. 6, our framework differs from traditional MCTS algorithms for game playing in the following ways:

1. The simulation is performed on the leaf node selected in the *Selection* module, instead of the child nodes opened in the *Expansion* one. Experimental results on real benchmarks indicate that this achieves a better performance for the QCT problem.
2. In game playing, the simulation result can be obtained only when the game is decided. In contrast, the reward of a move in our setting is collected during the execution of CNOT gates from the logic circuit. Consequently, in the *Simulation* module, we simulate only on a sub-circuit of the current logic circuit to improve efficiency.
3. We introduce a discount factor, which can be adjusted to better suit the problem setting, when back-propagating the simulated values.

### 3.1 Main modules

We now elaborate the five major modules one by one.

**Selection.** *Selection* is the iterated process to find an appropriate leaf node in the search tree to expand and simulate. It starts from the root node and, in each iteration, evaluates and picks one of the child nodes until a leaf node is reached.

The way we evaluate child nodes during *Selection* is critical to the performance of the whole algorithm. On one hand, if we only consider their values, the chance for exploring unpromising nodes will be too low and we can easily get stuck in a local minimum. On the other hand, if we always select nodes with a smaller visit count, the search will be too shallow and thus a large amount of time will be wasted in exploring inferior nodes. To get a balance between these two aspects, the following evaluation formula, similar to the well-known UCT (Upper Confidence Bound 1 applied to trees) [34], is introduced in our implementation to make a balanced evaluation among all child nodes  $\mathbf{s}'$  of  $\mathbf{s}$ :

$$\text{REW}(\mathbf{s}, \mathbf{s}') + \text{VAL}(\mathbf{s}') + c \sqrt{\frac{\log \text{VISIT}(\mathbf{s})}{\text{VISIT}(\mathbf{s}')}} \quad (2)$$

where  $c$  is a pre-defined parameter, and  $\text{VISIT}(\mathbf{s})$  is the number of times that  $\mathbf{s}$  has been visited. Intuitively, the first two terms in Eq. 2 correspond to the exploitation rate and the third the exploration rate in UCT. In each iteration of the *Selection* module, the node which maximises Eq. 2 is selected. The *Selection* module is presented in Alg. 1.

---

**Algorithm 1:**  $\text{Select}(\mathcal{T})$

---

**input** : A Monte Carlo search tree  $\mathcal{T}$ .  
**output:** A leaf node to expand and simulate.  
 $\mathbf{s} \leftarrow \text{root}(\mathcal{T});$   
 $\text{VISIT}(\mathbf{s}) \leftarrow \text{VISIT}(\mathbf{s}) + 1;$   
**while**  $\mathbf{s}$  is not a leaf node **do**  
     $\mathbf{s} \leftarrow$  the child node  $\mathbf{s}'$  of  $\mathbf{s}$  that maximises Eq. 2;  
     $\text{VISIT}(\mathbf{s}) \leftarrow \text{VISIT}(\mathbf{s}) + 1;$   
**return**  $\mathbf{s};$

---



**Expansion.** The goal of *Expansion* is to open all child nodes of a given leaf node by applying all relevant SWAP operations. Given a logic circuit  $C$  and a qubit mapping  $\tau$ , the set of *pertinent* SWAPs, denoted  $\mathcal{SWAP}_{C,\tau}$ , is the set of gates  $\text{SWAP}(v_i, v_j)$  such that either  $\tau^{-1}(v_i)$  or  $\tau^{-1}(v_j)$  appears in a gate in the current front layer of  $C$ , i.e.,

$$(v_i, v_j) \in E \text{ and } (\tau^{-1}(v_i) \in Q_0 \text{ or } \tau^{-1}(v_j) \in Q_0),$$

where  $Q_0$  is the set of logical qubits that are involved in the gates in  $\mathcal{L}_0(C)$ . To expand a selected node  $\mathbf{s} = (\tau, PC, LC)$ , only gates in  $\mathcal{SWAP}_{LC,\tau}$  will be applied to generate child nodes. This strategy has been widely used in quantum circuit transformation, see, e.g., [10, 8, 13]. In particular, several variants are introduced in FiDLS [15].

For each pertinent SWAP of  $\mathbf{s}$ , a new child node  $\mathbf{s}'$  will be generated. Furthermore, the reward  $\text{REW}(\mathbf{s}, \mathbf{s}')$  is as defined in Eq. 1 and both  $\text{VAL}(\mathbf{s}')$  and  $\text{VISIT}(\mathbf{s}')$  are set as 0. The details can be found in Alg. 2.

---

**Algorithm 2:** Expand( $\mathcal{T}, \mathbf{s}$ )

---

**input** : A Monte Carlo search tree  $\mathcal{T}$  and node  $\mathbf{s} = (\tau, PC, LC)$ .

**for** all  $\text{SWAP}(v_i, v_j)$  in  $\mathcal{SWAP}_{LC,\tau}$  **do**  
     $\tau' \leftarrow \tau[\tau^{-1}(v_i) \mapsto v_j, \tau^{-1}(v_j) \mapsto v_i];$   
     $C \leftarrow$  the set of all  $\tau'$ -executable gates in  $LC$ ;  
     $LC' \leftarrow LC$  with all gates in  $C$  deleted;  
     $PC' \leftarrow PC$  by adding  $\text{SWAP}(u_i, u_j)$  and all gates in  $C$ ;  
     $\mathbf{s}' \leftarrow (\tau', PC', LC')$ ;  
     $\text{VAL}(\mathbf{s}'), \text{VISIT}(\mathbf{s}') \leftarrow 0$ ;  
    Add  $\mathbf{s}'$  as a child node of  $\mathbf{s}$ ;  
     $\text{REW}(\mathbf{s}, \mathbf{s}') \leftarrow$  number of gates in  $C$ ;

---

**Simulation.** The objective here is to obtain a simulated score, serving as the initial long-term value  $\text{VAL}(\mathbf{s})$ , of the current state  $\mathbf{s}$  by simulation. In our implementation, we perform simulation on the first  $G_{\text{SIM}}$ , a predefined number, gates in the current logical circuit. While almost all existing QCT algorithms can be used for this purpose, for the sake of efficiency, a fast random simulation is designed in Alg. 3.

Given the current state  $\mathbf{s}$ , let  $N$  be, among all  $N_{\text{SIM}}$  (a predefined number) iterations, the minimal number of SWAP gates we have inserted until all the first  $G_{\text{SIM}}$  CNOT gates of  $LC(\mathbf{s})$  have been executed. Then the initial long-term value of  $\mathbf{s}$  is defined as

$$\text{VAL}(\mathbf{s}) = \gamma^{N/2} \cdot G_{\text{SIM}}, \quad (3)$$

where  $\gamma < 1$  is a predefined discount factor.

We next show how to do random simulation. Let  $C$  be a sub-circuit of  $LC(\mathbf{s})$  and  $\tau$  the current mapping. We write  $\mathcal{SWAP}_{C,\tau}$  for the set of pertinent SWAPs for  $C$  under  $\tau$ . For any  $h \in \mathcal{SWAP}_{C,\tau}$ , its *impact factor* is defined as

$$\text{IF}(h) := f\left(\sum_{g \in \mathcal{L}_0(C)} \text{SCOST}(g, \tau) - \sum_{g \in \mathcal{L}_0(C)} \text{SCOST}(g, \tau')\right)$$

where  $\tau'$  is the mapping obtained from  $\tau$  after applying  $h$  and  $f$  the scaling function defined as

$$f(x) = \begin{cases} 0, & \text{if } x < 0 \\ 0.001, & \text{if } x = 0 \\ x, & \text{if } x > 0 \end{cases}$$

Furthermore,  $\text{SCOST}(g, \tau)$  is the *swap cost* of  $g = \text{CNOT}(q_j, q_k)$  with respect to  $\tau$ , which is defined to be the shortest distance between the physical qubits  $\tau(q_j)$  and  $\tau(q_k)$  in the architecture graph. Then, a probability distribution is obtained as follows

$$P(X = h) = \frac{\text{IF}(h)}{\sum \{\text{IF}(h') \mid h' \in \mathcal{SWAP}_{C,\tau}\}}, \quad (4)$$

through which a SWAP operation can be sampled from  $\mathcal{SWAP}_{C,\tau}$  and used to execute gates from  $LC$ . Note that this simulation process will be repeated for  $N_{\text{SIM}}$ , also a predefined parameter, times to obtain the best score.

---

**Algorithm 3:** Simulate( $\mathcal{T}, \mathbf{s}$ )

---

**input** : A Monte Carlo search tree  $\mathcal{T}$  and node  $\mathbf{s} = (\tau, PC, LC)$ .  
 $N \leftarrow \infty$ ;  
**do**  
     $C \leftarrow$  circuit with the first  $G_{\text{SIM}}$  gates in  $LC$ ;  
     $n \leftarrow 0$ ;  $\tau' \leftarrow \tau$ ;  
    **while**  $C$  is not empty **do**  
        Sample  $h$  from  $\mathcal{SWAP}_{C,\tau'}$  according to the probability distribution in Eq. 4;  
         $\tau' \leftarrow \tau'$  by applying  $h$ ;  
         $C \leftarrow C$  with all  $\tau'$ -executable gates deleted;  
         $n \leftarrow n + 1$ ;  
    **if**  $n < N$  **then**  
         $N \leftarrow n$ ;  
**for**  $N_{\text{SIM}}$  times;  
 $\text{VAL}(\mathbf{s}) \leftarrow \gamma^{N/2} \cdot G_{\text{SIM}}$ ;

---

Another issue which deserves explanation is the way we compute the simulated score (or, the initial value) for state  $\mathbf{s}$  in Eq. 3. In particular, one may wonder why the exponent is  $N/2$  instead of  $N$ ? The intuitive meaning of this definition is as follows. Although these  $G_{\text{SIM}}$  gates are executed in different steps during the simulation, for simplicity, we suppose they are all executed right at the middle point  $\mathbf{s}'$  which is the  $N/2$ -generation son of  $\mathbf{s}$ . Then the reward collected at the transition to  $\mathbf{s}'$  from its parent is exactly  $G_{\text{SIM}}$ . Note that every edge along the path from  $\mathbf{s}$  to the parent of  $\mathbf{s}'$  has zero reward. Thus, we need only backpropagate the reward collected at  $\mathbf{s}'$  upwards with discount factor  $\gamma$ . This gives the simulated score  $\gamma^{N/2} \cdot G_{\text{SIM}}$  for  $\mathbf{s}$  as specified in Eq. 3. Real benchmark experiments also confirm that the current choice performs better than simply letting  $\text{VAL}(\mathbf{s})$  be the sum of all the (discounted) rewards collected during the actual execution of these  $G_{\text{SIM}}$  CNOT gates.

**Backpropagation.** The *Backpropagation* module updates the values of ancestors of the just simulated node in the search tree. More precisely, the value of node  $\mathbf{s}$  in the propagated path will be updated as

$$\text{VAL}(\mathbf{s}) \leftarrow \max \{ \text{VAL}(\mathbf{s}), \gamma \cdot [\text{REW}(\mathbf{s}, \mathbf{s}') + \text{VAL}(\mathbf{s}')] \}, \quad (5)$$

in which  $\mathbf{s}'$  is the child node of  $\mathbf{s}$  on the path. This reflects the intuitive meaning of  $\text{VAL}(\mathbf{s})$  discussed at the beginning of this section. The implementation is shown in Alg. 4.

---

**Algorithm 4:** Backpropagate( $\mathcal{T}, \mathbf{s}$ )

---

**input** : A Monte Carlo search tree  $\mathcal{T}$  and node  $\mathbf{s}$ .  
**while**  $\mathbf{s} \neq \text{root}(\mathcal{T})$  **do**  
     $\mathbf{s}' \leftarrow$  parent node of  $\mathbf{s}$ ;  
     $\text{VAL}(\mathbf{s}') \leftarrow \max \{ \text{VAL}(\mathbf{s}'), \gamma \cdot [\text{REW}(\mathbf{s}', \mathbf{s}) + \text{VAL}(\mathbf{s})] \}$ ;  
     $\mathbf{s} \leftarrow \mathbf{s}'$ ;

---

**Decision.** This module, depicted in Alg. 5, decides the best move from the root node  $rt$  and updates the search tree with the subtree rooted at the best child node of  $rt$ .

### 3.2 Combine Everything Together

Finally, we combine all modules together as in Alg. 6 to form the MCTS framework for QCT. Note that, to ensure the reliability of the *Decision* module, a sufficiently large number ( $N_{\text{BP}}$ , a predefined parameter) of

---

**Algorithm 5:** Decide( $\mathcal{T}$ )

---

**input** : A Monte Carlo search tree  $\mathcal{T}$ .  
     $rt \leftarrow \text{root}(\mathcal{T})$ ;  
     $\mathbf{s} \leftarrow$  child node of  $rt$  with the highest  $\text{REW}(rt, \mathbf{s}) + \text{VAL}(\mathbf{s})$ ;  
     $\mathcal{T} \leftarrow$  the subtree of  $\mathcal{T}$  rooted at  $\mathbf{s}$ ;

---

*Selection*, *Expansion*, *Simulation*, and *Backpropagation*, should be performed to get a good estimation of the values of relevant states.

Due to the stochastic nature of our algorithm, there is a negligible but still positive possibility that at certain iteration of the while loop in Alg. 6, even the best child node derived from the *Decision* module cannot execute any new gate. To guarantee termination in this extreme case, a *fallback* mechanism, which has been widely used in the literature (cf. [7]), is adopted. Specifically, if no CNOTs have been executed after  $|V|$  consecutive *Decisions* and the current root node is  $(\tau, PC, LC)$ , then we choose a CNOT from  $\mathcal{L}_0(LC)$  with minimum swap cost with respect to  $\tau$ , and insert the corresponding SWAP gates to  $PC$  so that progress will be made by executing this chosen CNOT. For the sake of readability, the fallback module is omitted in Alg. 6.

---

**Algorithm 6:** Quantum circuit transformation based on Monte Carlo tree search

---

**input** : An architecture graph  $AG$ , a logical circuit  $LC$ , and an initial mapping  $\tau_{ini}$ .

**output**: A physical circuit satisfying the connectivity constraints in  $AG$ .

$PC \leftarrow$  the circuit consisting of all executable gates in  $LC$  under  $\tau_{ini}$ ;

$LC \leftarrow LC$  with gates in  $PC$  deleted;

$\mathbf{s} \leftarrow (\tau_{ini}, PC, LC)$ ;

$\text{VAL}(\mathbf{s}), \text{VISIT}(\mathbf{s}) \leftarrow 0$ ;

$\mathcal{T} \leftarrow$  a search tree with a single (root) node  $\mathbf{s}$ ;

**while**  $LC(\mathbf{s}) \neq \emptyset$  **do**

**do**

$\mathbf{s} \leftarrow \text{Select}(\mathcal{T})$ ;

$\text{Expand}(\mathcal{T}, \mathbf{s})$ ;

$\text{Simulate}(\mathcal{T}, \mathbf{s})$ ;

$\text{Backpropagate}(\mathcal{T}, \mathbf{s})$ ;

**for**  $N_{BP}$  *times*;

$\text{Decide}(\mathcal{T})$ ;

$\mathbf{s} \leftarrow \text{root}(\mathcal{T})$ ;

**return**  $PC(\mathbf{s})$

---

### 3.3 Complexity Analysis

This subsection is devoted to a rough analysis of the complexity of our algorithm. Suppose  $AG = (V, E)$  and the input logical circuit  $LC = (Q, C)$ . Among the five main modules presented in subsection 3.1, the most expensive ones are *Selection*, *Expansion*, and *Simulation*. We analyse their complexity separately as follows.

**Selection.** The complexity of this module depends on the depth of the search tree. In the worst case, each of the  $N_{BP}$  iteration in the **do** loop of Alg. 6 increases the depth by 1. Taking into account the fallback introduced in the last subsection, the depth of the search tree is at most  $N_{BP} \cdot |V|$ . As each node has at most  $|E|$  children, the overall complexity for this module is  $O(N_{BP} \cdot |V| \cdot |E|)$ .

**Expansion.** There are at most  $|E|$  pertinent SWAP gates available to create new nodes, and for each new one, at most  $|C|$  gates need to be checked to see whether they are executable. Thus the time complexity is  $O(|E| \cdot |C|)$ . Here  $|C|$  denotes the number of gates in  $C$ .

**Simulation.** Computing the probability distribution in Eq. 4 takes time  $O(|E| \cdot |V|)$ . To guarantee termination, the while loop will be aborted if no gates have been executed after  $|V|$  consecutive iterations. Hence, the complexity of this module is  $O(|E| \cdot |V|^2 \cdot G_{SIM} \cdot N_{SIM})$ .

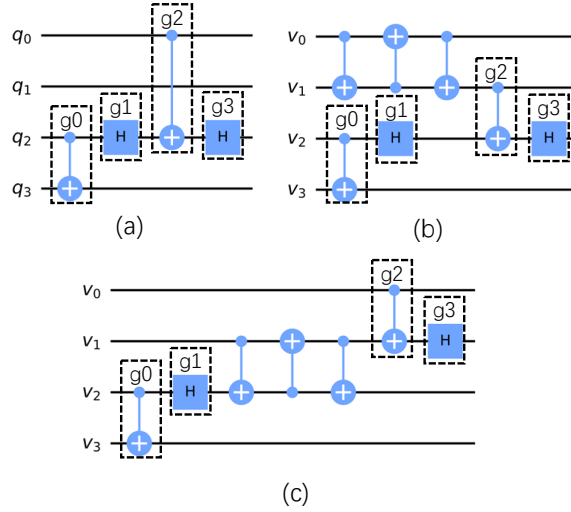


Figure 7: An input quantum circuit (a) and two functionally equivalent physical circuits, (b) and (c), that are executable on IBM Q20 with the naive initial mapping.

Finally, note that in the worst case, all gates from  $C$  are executed by the fallback mechanism which is invoked after every  $|V|$  iterations. Hence, the *Sel-Exp-Sim-BP* modules will be run for at most  $|C| \cdot |V| \cdot N_{BP}$  times, and the overall time complexity of our algorithm is

$$O(|C| \cdot |V| \cdot N_{BP} \cdot |E| \cdot [N_{BP} \cdot |V| + |C| + |V|^2 \cdot G_{SIM} \cdot N_{SIM}]),$$

or  $O(|C| \cdot |V| \cdot |E| \cdot (|C| + |V|^2))$  when the parameters are regarded as constants.

## 4 Depth Optimisation

QPUs in the NISQ era also suffer from limited coherence time, meaning that the depth of the output physical circuit is also an important criterion for optimising the circuit transformation process. In this section, we propose MCTS-Depth, which is adapted from the MCTS-Size algorithm presented in the previous section by introducing two minor changes, to further reduce the depth of the output circuit.

Recall that in MCTS-Size we have removed all single-qubit gates because they have no effect when the QCT objective is to minimise the number of inserted SWAP gates. However, as shown in Example 4, this is not the case as far as circuit depth is concerned. In this paper, we adopt a simple strategy to deal with these gates: whenever an executable CNOT  $g$  is removed from the logical circuit and added to the physical circuit in *Expansion*, all single-qubit gates after  $g$  and before any other CNOT that directly depends on  $g$  will be greedily added to the physical circuit.

**Example 4.** Suppose the quantum (logical) circuit to be transformed by MCTS-Depth is specified as in Fig. 7(a). Assume that the target QPU is IBM Q20 and we take the initial mapping to be the naive one. As the CNOT  $g_0$  is directly executable,  $g_0$  and the single-qubit gate  $g_1$  are immediately added to the physical circuit. To make  $g_2$  executable, we can insert a SWAP either between physical qubits  $v_0$  and  $v_1$  (cf. Fig. 7(b)) or between  $v_1$  and  $v_2$  (cf. Fig. 7(c)). The depth overhead brought by adding SWAP( $v_0, v_1$ ) and SWAP( $v_1, v_2$ ) are, respectively, 1 and 3, after decomposing each SWAP into 3 CNOTs.

As shown in Example 4, different SWAP gates may incur different depth overheads. Let  $\mathbf{s} = (\tau, PC, LC)$  be the current state and  $\mathbf{s}' = (\tau', PC', LC')$  the child state corresponding to some SWAP. As each SWAP is implemented as three consecutive CNOTs, the depth overhead, written  $I_{\mathbf{s}'}$ , is an integer between 0 and 3. That is, a SWAP may incur 0, 1, 2, or 3 extra layers. The precise value of  $I_{\mathbf{s}'}$  is calculated as the depth difference of  $PC'$  and  $PC$ , where the executed single-qubit gates are properly added back. Apparently, we prefer SWAPs

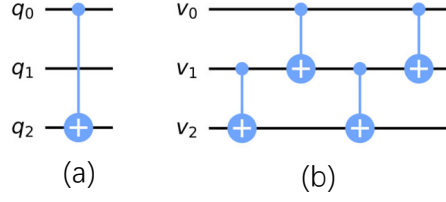


Figure 8: Take  $AG$  to be that of IBM Q20 and the initial mapping  $\tau$  be naive. (a) A logical circuit with only one gate  $\text{CNOT}(q_0, q_2)$ . (b) A remote CNOT implementation of  $\text{CNOT}(q_0, q_2)$ .

with smaller  $I_{s'}$ . This motivates us to replace the discount factor  $\gamma$  in Eq. 5 for MCTS-Size with  $\gamma^{I_{s'}}$  and obtain the following value-update rule for MCTS-Depth:

$$\text{VAL}(\mathbf{s}) \leftarrow \max\{\text{VAL}(\mathbf{s}), \gamma^{I_{s'}} \cdot [\text{REW}(\mathbf{s}, \mathbf{s}') + \text{VAL}(\mathbf{s}')]\} \quad (6)$$

Another modification is applied to the definition of the initial long-term value of a state  $\mathbf{s}$  in the simulation process, given in Eq. 3, where it uses  $N$ , the minimal number of SWAP gates required during all  $N_{\text{SIM}}$  simulations, as an important index. Apparently, in order to reduce depth, it is more meaningful to replace  $N$  with  $M$ , the minimal depth overhead of all  $N_{\text{SIM}}$  simulations. That is, in MCTS-Depth, Eq. 3 is replaced with

$$\text{VAL}(\mathbf{s}) = \gamma^{M/2} \cdot G_{\text{SIM}} \quad (7)$$

and the second last line of Alg. 3 is replaced with

$$\text{VAL}(\mathbf{s}) \leftarrow \gamma^{M/2} \cdot G_{\text{SIM}}.$$

It is clear that these modifications do not affect the complexity analysis given in Sec. 3.3.

## 5 Incorporating Remote CNOT

In above, we have seen how a circuit can be transformed by inserting SWAPs. This is sometimes not desirable as the mapping will change with the inserted SWAPs (cf. Example 5 below). Several transformers (including the current version of t|ket>) suggest using remote CNOT operations (also known as bridge gates) to execute CNOT gates whose two qubits in the current mapping are not neighbours (i.e., remote). In this section, we show how remote CNOTs can be incorporated into our MCTS-based algorithms.

Let  $\tau$  be the current mapping and  $g = \text{CNOT}(q, q')$ . If the two physical qubits  $\tau(q)$  and  $\tau(q')$  are not neighbours in the target  $AG$ , we may replace  $g$  with a sequence of CNOT gates, written  $\mathcal{R}_\tau(g)$ , which are executable and functionally equivalent to  $g$ . Fig. 8(b) shows the special case when the distance of  $\tau(q)$  and  $\tau(q')$  in  $AG$  is 2. More general construction can be found in [39].

**Example 5.** Consider the circuit shown in Fig. 4 (left). Except  $g_0$ , every CNOT in the circuit can be executed by the naive mapping. If only SWAPs are allowed, we need to insert a SWAP to execute  $g_0$ . As a consequence, the mapping is changed and at least one of the other CNOTs are not executable and we need to insert another SWAP, which results in a size overhead of at least six! However,  $g_0$  can be executed by implementing it as a remote CNOT depicted in Fig. 8(b) and, after that, the other CNOTs can be immediately executed, which gives an overhead of three!

To extend our MCTS algorithms with remote CNOT, we need only modify *Expansion* and *Backpropagation*. Starting from a state/node  $\mathbf{s} = (\tau, PC, LC)$ , besides all relevant SWAPs as used in Alg. 2, we also consider all  $g = \text{CNOT}(q, q')$  if  $g$  is in the first layer of  $LC$  and the distance of  $\tau(q)$  and  $\tau(q')$  in  $AG$  is between 2 and some fixed integer  $d$ . We then may replace  $g$  with a CNOT sequence  $\mathcal{R}_\tau(g)$  along the shortest path connecting  $\tau(q)$  and  $\tau(q')$  if desirable. As remote CNOTs and SWAPs may incur different size and depth overheads, a modified value-update rule like Eq. 6 is used during *Backpropagation* if  $\mathbf{s}' = (\tau', PC', LC')$  is the child node of  $\mathbf{s}$  derived by a remote CNOT implementation of  $g$ . More precisely, for MCTS-Size,  $I_{s'}$  is defined as  $(|\mathcal{R}_{\tau'}(g)| - 1)/3$ . The

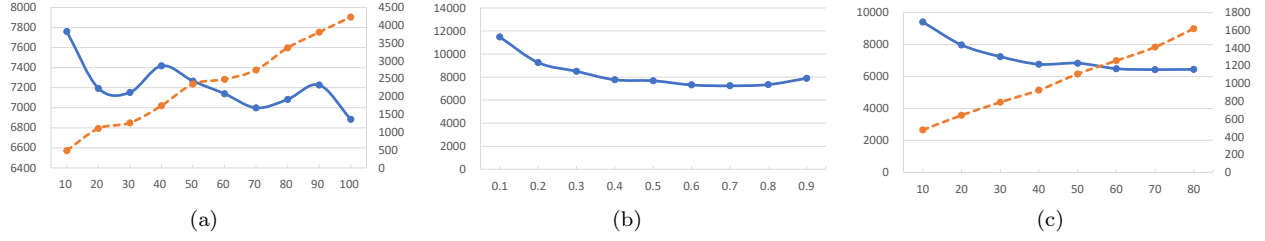


Figure 9: Evaluation of the performance of MCTS-Size on IBM Q20 for different parameter settings: (a)  $N_{BP}$ , (b)  $\gamma$ , and (c)  $G_{SIM}$ , where the vertical axes on the left and right in each sub-figure represent the aggregated number of added CNOTs in output circuits (blue lines) and running time (seconds, orange dashed lines), respectively. All data is aggregated from a small set of benchmarks with 11 circuits and 26,676 CNOT gates in total and initial mappings are the same as those used in SAHS [13].

intuition behind this is that the sub-circuit  $\mathcal{R}_{\tau'}(g)$  we used to replace  $g$  brings a size overhead of  $|\mathcal{R}_{\tau'}(g)| - 1$  in terms of CNOTs, which translates to  $(|\mathcal{R}_{\tau'}(g)| - 1)/3$  in terms of SWAPs. For MCTS-Depth,  $I_{s'}$  is set as the depth overhead brought by adding gates in  $\mathcal{R}_{\tau'}(g)$  to the physical circuit in state  $s'$ .

To conclude this section, we point out that the remote CNOT approach does not always give better result than the SWAP-based approach. This is because inserting SWAPs changes the mapping, which is sometimes desirable as the new mapping may execute more later CNOTs. Consider again the circuit in Fig. 4 (left). If the CNOT gate  $g_3$  were applied on  $q_0$  and  $q_2$ , then inserting  $\text{SWAP}(v_0, v_1)$  (i.e. three CNOTs) suffices to solve all gates in the circuit, while remote implementation of both  $g_0$  and  $g_3$  would introduce an overhead of six CNOTs. In practice, however, it might not be easy to decide which approach is preferable. Thus we provide both of them as possible choices. In Sec. 6 we will evaluate its impact for two AGs.

## 6 Programming and Benchmarks

To evaluate our approach, we compare it with three state-of-the-art algorithms proposed in the literature [13, 15, 12]. As the choice of initial mappings may sometimes influence the performance of QCT algorithms, to make a fair comparison, we always take the same initial mappings in their original design if available. We use Python as our main programming language and IBM Qiskit [4] as the auxiliary environment to implement our algorithms<sup>4</sup>. For efficiency, the *Simulation* module is implemented in C++. All experimental results reported here are obtained by choosing the best one from 5 trials. Due to space limitations, we only provide summarised results here. Readers are referred to the online Appendix for detailed empirical results.

In our evaluation, we selected a set of 114 benchmark circuits, with a sum of 554,497 gates (including 248,553 CNOTs) and a sum of 303,469 depths, which are taken from [10] and widely used in evaluating circuit transformation algorithms by, e.g., [12, 15, 13, 8].

Our MCTS-based QCT algorithms have a couple of parameters to be determined before actual running:

- $N_{BP}$  (repeated times for the *Sel-Exp-Sim-BP* modules before each *Decision* ),
- $c$  (the exploration parameter used in Eq. 2),
- $G_{SIM}$  (the size of sub-circuit used in simulation),
- $N_{SIM}$  (the number of simulations),
- $\gamma$  (the discount ratio), and
- $d$  (the maximum distance allowed for remote CNOT).

<sup>4</sup>Source code is available at <https://github.com/BensonZhou1991/Circuit-Transformation-via-Monte-Carlo-Tree-Search>

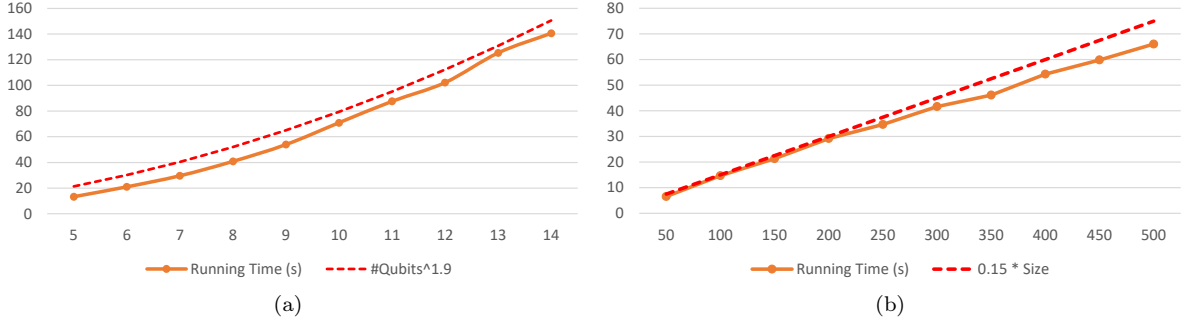


Figure 10: Evaluations of the performance of MCTS-Size on IBM Q20 by comparing the average running time (seconds, orange line) with (a): number of logical qubits, and (b): number of CNOTs of the input circuits, where each circuit in (a) contains 500 CNOTs and each circuit in (b) has 10 qubits, and each data point denotes the average value of 10 randomly generated quantum circuits with naive initial mappings.

To help determine these parameters for IBM Q20, we selected a small subset of 11 benchmark circuits, which contains in total 26,676 CNOTs. To get a good balance between performance and running time, we empirically set

$$N_{BP} = c = 20, G_{SIM} = 30, N_{SIM} = 500, \text{ and } \gamma = 0.7.$$

We adopt the same parameter setting for the other proposed algorithms, and set  $d = 2$  for MCTS-Size and MCTS-Depth.

We have shown in Sec. 3.3 that our algorithm runs in time polynomial in all relevant parameters. To further demonstrate the running time in practice, we randomly generate two sets of 10 quantum circuits. In one set, each circuit has 500 CNOTs, and the number of logical qubits ranges from 5 to 14. In the other, each circuit has 10 qubits, and the number of CNOTs ranges from 50 to 500. We transform all these circuits via MCTS-Size on IBM Q20, and record the average running time for each circuit set. As shown in Fig. 10, the real time cost is roughly the 1.9th power in the number of qubits and linear (with slope being about 0.15) in the number of CNOTs, indicating that our algorithm is practically scalable.

Now we compare MCTS-Size with SAHS [13], FiDLS [15], and  $t|ket\rangle$  [12] on IBM Q20 over the 114 benchmark circuits. The results are summarised in Table 1, where columns 2 & 3 represent aggregated numbers of added CNOTs (each SWAP is decomposed into 3 CNOTs) obtained from other methods and MCTS-Size when using their initial mappings, respectively. Besides, the ‘improvement’ is defined as  $(n_{comp} - n_{ours})/n_{comp}$ , with  $n_{comp}$  and  $n_{ours}$  being the total numbers of CNOT gates added by the compared algorithm and ours, respectively, in transforming the 114 circuits. A similar definition for ‘Improvement’ is used in the rest of the paper.

Table 1: Summarised results for the large benchmark set with 114 circuits

	CNOT Added Others	CNOT Added MCTS-Size	Improvement
SAHS	116487	73758	36.68%
Topg. FiDLS	107406	74763	30.39%
Weig. FiDLS	105645	75126	28.89%
$t ket\rangle$	238170	77544	59.24%

From Table 1, we can see that MCTS-Size achieves a conspicuous improvement of 36.68% on average when compared with SAHS (by using the same initial mappings as SAHS). In [15], two techniques for initial mappings, topgraph (topg.) and weighted graph (weig.), are proposed with FiDLS. Our algorithm has a consistent improvement, 30.39% for the topgraph initial mappings and 28.89% for the weighted graph ones. The version of  $t|ket\rangle$  we compare with is 0.7.0.<sup>5</sup> As the initial mappings of  $t|ket\rangle$  are not directly available, we use naive mappings as the initial mappings in the experiments. For fair and pure comparison of the routing

<sup>5</sup><https://cqcl.github.io/pytket/build/html/index.html>

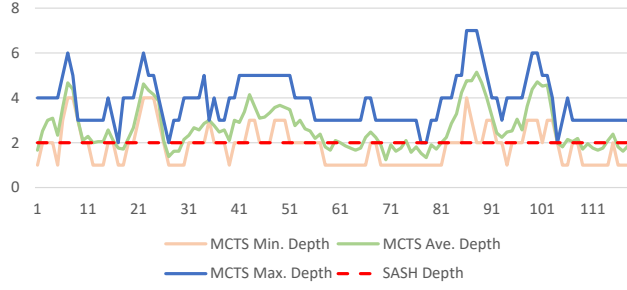


Figure 11: Search depth (for *Selection* before each *Decision*) of MCTS-Size for circuit ‘misex1\_241’. The horizontal and vertical axis represent rounds for *Decision* and search depth, respectively.

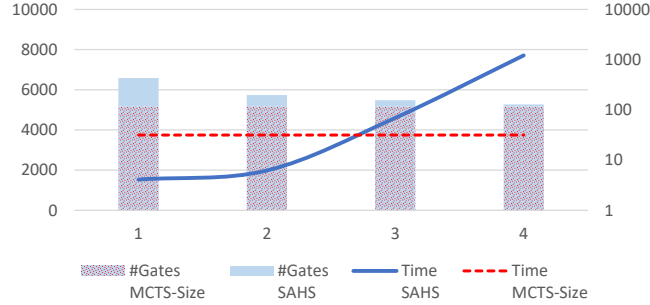


Figure 12: The benefit brought by increasing the search depth in SAHS [13] for circuit ‘misex1\_241’. The horizontal axis and vertical axes on the left and right represent search depth, number of gates in the output circuit and running time (seconds), respectively.

abilities, we also disabled the postmapping optimisation of  $t|ket\rangle$ . As can be seen from the last row of Table 1, the gate overhead of  $t|ket\rangle$  is above 3 times of ours (also with naive initial mappings). It is worth noting that, on this benchmark set, MCTS-Size still performs well even with naive initial mappings; the overhead compared with the best result is only 5.13% (77,544 vs. 73,758).

For MCTS-Size, we also record the search depth for each use of the *Selection* module and calculate the minimum, average, and maximum depth before each *Decision* process. As shown in Fig. 11, the maximum depth can easily exceed that of SAHS [13], which is set to 2. Actually, in most of the time it is more than 3, meaning that our algorithm has better ability of exploring the unknown state. Note that it is claimed in [13] that the size of output physical circuits can be further decreased by increasing the search depth, with the cost of more time consumption. Fig. 12 depicts a comparison of the output circuit size as well as the running time of MCTS-Size and SAHS on the example circuit ‘misex1\_241’ with 4,813 gates, where for SAHS, the search depth varies from 1 to 4. It shows that MCTS-Size outperforms SAHS in the output circuit size even when the search depth of SAHS is set to 4. However, in this case, the running time of SAHS is over 20 minutes, while MCTS-Size only needs 31 seconds.

Now we compare MCTS-Depth with both MCTS-Size and  $t|ket\rangle$  on the benchmark set in terms of the total depth overhead. As the initial mappings used by  $t|ket\rangle$  are not directly available, we adopt the naive mapping as the initial mapping for all three algorithms. It is surprise that on IBM Q20 the initial mappings selected by  $t|ket\rangle$  are, on average, not better than the naive mappings (238,170 vs. 237,471 added CNOTs and 238,051 vs. 236,312 added depths). As can be seen from Table 2, MCTS-Depth is able to improve the depth performance steadily for both tested AGs when compared to MCTS-Size, which confirms the utility of our modifications in Sec. 4. We note that the improvements of Alg. X against Alg. Y in Table 2 are calculated as  $(n_Y - n_X)/n_Y$  with  $n_Y$  ( $n_X$ , resp.) being either the sum of the added CNOTs or the sum of the added depths by Alg. Y (Alg. X, resp.). When compared with  $t|ket\rangle$ , for IBM Q20, both MCTS-Size and MCTS-Depth have a great advantage, with about 75% and 84% improvement; for Grid  $5 \times 4$ , however, their advantages are not so remarkable. The main reason is perhaps due to the fact that IBM Q20 supports more qubit connections (and has a smaller



diameter) than Grid  $5 \times 4$ , which enables the MCTS-based algorithms to find a good solution without going much deeper for IBM Q20. Another reason may be that  $t|ket\rangle$  performs really well on grid-like AGs.

Finally, we discuss the improvement brought by introducing remote CNOT. We empirically evaluated the impact of remote CNOT in our MCTS-based algorithms and  $t|ket\rangle$ . The results are summarised in Table 2, where for an algorithm A, A+r denotes the algorithm with remote CNOT enabled. For IBM Q20, the improvements brought by introducing remote CNOT are almost negligible, and sometimes even degraded. For Grid  $5 \times 4$ , however, the improvements are quite significant. Compared to  $t|ket\rangle$ , our algorithms have gained an improvement of 28% in size (MCTS-Size+r) and an improvement of 42% in depth (MCTS-Depth+r), while  $t|ket\rangle$ +r has a 4% improvement in size and a 14% improvement in depth.

Table 2: Summarised results of the proposed algorithms and  $t|ket\rangle$  over the large benchmark set with 114 circuits

AG	Method	CNOT Added	Depth Added	Size Imp.	Depth Imp.
IBM Q20	$t ket\rangle$	237471	236312	-	-
	$t ket\rangle$ +r	273420	238661	-15.14%	-0.99%
	MCTS-Size	79743	58602	66.42%	75.20%
	MCTS-Size+r	79275	59857	66.62%	74.67%
	MCTS-Depth	151530	37794	36.19%	84.01%
	MCTS-Depth+r	147972	37138	37.69%	84.28%
Grid $5 \times 4$	$t ket\rangle$	383409	368109	-	-
	$t ket\rangle$ +r	367815	314148	4.07%	14.66%
	MCTS-Size	356091	359240	7.13%	2.41%
	MCTS-Size+r	275274	263811	28.20%	28.33%
	MCTS-Depth	514311	292050	-34.14%	20.66%
	MCTS-Depth+r	392349	211421	-2.33%	42.57%

Although the current benchmark set is widely used in QCT papers, functions implemented by some circuits in it are not directly relevant to quantum computing. To evaluate the proposed algorithms under ‘real’ quantum circuits, we also extracted a set of 173 quantum circuits from the quantum algorithm library in Qiskit with a sum of 603,654 gates (including 260,589 CNOTs) and a sum of 413,734 depths<sup>6</sup>. We evaluated both our MCTS-based QCT algorithms and  $t|ket\rangle$  on IBM Q20 and the initial mappings are set to be naive. The results are recorded in Table 3, and it shows that the improvements of our algorithms to  $t|ket\rangle$  are still significant and consistent compared to the results in Table 2.

<sup>6</sup>The QASM files of these circuits are available at [https://github.com/BensonZhou1991/quantum\\_circuit\\_benchmark](https://github.com/BensonZhou1991/quantum_circuit_benchmark)

Table 3: Summarised results of the proposed algorithms and  $t|ket\rangle$  over quantum circuits extracted from Qiskit library

AG	Method	CNOT Added	Depth Added	Size Imp.	Depth Imp.
IBM Q20	Pytket	101304	91730	-	-
	Pytket+r	156774	121734	-54.76%	-32.71%
	MCTS-Size	41010	41826	59.52%	54.40%
	MCTS-Size+r	38607	49012	61.89%	46.57%
	MCTS-Depth	64992	27237	35.84%	70.31%
	MCTS-Depth+r	60333	31300	40.44%	65.88%

## 7 Conclusion

In this paper, an MCTS framework is proposed for the quantum circuit transformation problem, which aims at minimising either the size or the depth overhead to transform an ideal logical circuit to a physical one executable on a QPU with connectivity constraints. For this purpose, a scoring mechanism (cf. Eq.s 5 and 6) is designed which takes into account both the short-term reward of introducing a SWAP and a long-term value obtained by random simulations. Furthermore, when backpropagating rewards collected by states to their ancestors, a discount factor is introduced to guide the algorithm towards a cheapest path to a goal state. The MCTS-based algorithms, viz., MCTS-Size and MCTS-Depth, run in polynomial time with respect to all relevant parameters. With six parameters, they are very flexible in meeting different optimisation objectives, can stop whenever a preassigned resource limit is reached, and search much deeper than existing algorithms. Empirical results on extensive realistic circuits on IBM Q20 confirmed that MCTS-Size (MCTS-Depth, resp.) can reduce, on average, the CNOT (depth, resp.) overhead by at least 75% (84%, resp.) when compared with  $t|ket\rangle$ , an industrial level product. We also compared MCTS-Depth with the new algorithm proposed in [40], which aims at minimising the depth of the output circuit. Evaluation on IBM Q20 and 26 benchmark circuits used in [40] shows that MCTS-Depth performs consistently better and can reduce on average the depth overhead by 67% when compared with the approximate algorithm in [40].

When designing QCT algorithms, we assume that logical circuits are transformed into executable physical circuits by inserting ancillary CNOTs stepwise. This is very different with algorithms which try to ‘re-compile’ part of or the whole logical circuit to make the CNOTs in the newly compiled one satisfying the connectivity constraints, e.g., [41]. Combination of the two approaches may generate functional equivalent physical circuits with lower depth.

Recently, Tan and Cui [42] proposed a random circuit library QUEKO for evaluating the optimality of quantum circuit transformers, which contains circuits with known optimal depth overhead. We evaluated MCTS-Depth on QUEKO and the results show a total score of 2.88 (meaning the ratio of the total depths of the output and input circuits), which is, though better than that of  $t|ket\rangle$  (3.76), is still too far from the optimal ratio, viz. 1. This is partially due to that we used naive initial mappings, instead of the optimal mappings, e.g., those found by subgraph isomorphism [15]. On the other hand, it suggests that there is still much room to improve the implementation of our algorithms. This is the first problem we intend to attack for future studies. Second, parameters presented in our algorithms are QPU-dependent, and a careful study of their correlation may provide a better insight on how to choose them in practice. Third, more objectives, e.g., fidelity and error rate, should be included in evaluating the quality of output physical circuits. Last but not least, it is promising to develop a parallelised implementation of our MCTS-based algorithms in a multi-thread way, where hundreds or thousands computational processes can run in parallel and share the same memory. The success implementation of this parallelised MCTS framework could help us get even better results (by going deeper) more quickly.

## 8 Acknowledgments

This work was supported by the National Key R&D Program of China (Grant No. 2018YFA0306704) and the Australian Research Council (Grant No. DP180100691).

## References

- [1] F. Arute, K. Arya, R. Babbush, D. Bacon, J. C. Bardin, R. Barends, R. Biswas, S. Boixo, F. G. Brandao, D. A. Buell, et al., Quantum supremacy using a programmable superconducting processor, *Nature* 574 (7779) (2019) 505–510.
- [2] T. Häner, D. S. Steiger, K. Svore, M. Troyer, A software methodology for compiling quantum programs, *Quantum Science and Technology* 3 (2) (2018) 020501.
- [3] S. Sivarajah, S. Dilkes, A. Cowtan, W. Simmons, A. Edgington, R. Duncan,  $t|ket\rangle$ : a retargetable compiler for nisq devices, *Quantum Science and Technology* 6 (1) (2020) 014003.

- [4] G. A. et al., Qiskit: An open-source framework for quantum computing (2019). doi:10.5281/zenodo.2562110.
- [5] D. Maslov, S. M. Falconer, M. Mosca, Quantum circuit placement: Optimizing qubit-to-qubit interactions through mapping quantum circuits into a physical experiment, in: Proceedings of the 44th Design Automation Conference, DAC 2007, San Diego, CA, USA, June 4-8, 2007, IEEE, 2007, pp. 962–965. doi:10.1145/1278480.1278717.  
URL <https://doi.org/10.1145/1278480.1278717>
- [6] D. Cheung, D. Maslov, S. Severini, Translation techniques between quantum circuit architectures, in: Workshop on Quantum Information Processing, 2007.
- [7] A. M. Childs, E. Schoute, C. M. Unsal, Circuit transformations for quantum architectures, in: 14th Conference on the Theory of Quantum Computation, Communication and Cryptography, 2019.
- [8] G. Li, Y. Ding, Y. Xie, Tackling the qubit mapping problem for NISQ-era quantum devices, in: Proceedings of the Twenty-Fourth International Conference on Architectural Support for Programming Languages and Operating Systems, ACM, 2019, pp. 1001–1014.
- [9] M. A. Nielsen, I. Chuang, Quantum computation and quantum information, Cambridge University Press, 2002.
- [10] A. Zulehner, A. Paler, R. Wille, An efficient methodology for mapping quantum circuits to the ibm qx architectures, IEEE Transactions on Computer-Aided Design of Integrated Circuits and Systems 38 (7) (2018) 1226–1236.
- [11] A. Paler, On the influence of initial qubit placement during NISQ circuit compilation, in: International Workshop on Quantum Technology and Optimization Problems, Springer, 2019, pp. 207–217.
- [12] A. Cowtan, S. Dilkes, R. Duncan, A. Krajenbrink, W. Simmons, S. Sivarajah, On the qubit routing problem, in: 14th Conference on the Theory of Quantum Computation, Communication and Cryptography, 2019.
- [13] X. Zhou, S. Li, Y. Feng, Quantum circuit transformation based on simulated annealing and heuristic search, IEEE Transactions on Computer-Aided Design of Integrated Circuits and Systems 39 (12) (2020) 4683–4694. doi:10.1109/TCAD.2020.2969647.
- [14] M. Y. Siraichi, V. F. d. Santos, C. Collange, F. M. Q. Pereira, Qubit allocation as a combination of subgraph isomorphism and token swapping, Proceedings of the ACM on Programming Languages 3 (OOPSLA) (2019) 1–29.
- [15] S. Li, X. Zhou, Y. Feng, Qubit mapping based on subgraph isomorphism and filtered depth-limited search, IEEE Transactions on Computers (accepted). doi:10.1109/TC.2020.3023247.
- [16] A. Lye, R. Wille, R. Drechsler, Determining the minimal number of swap gates for multi-dimensional nearest neighbor quantum circuits, in: The 20th Asia and South Pacific Design Automation Conference, IEEE, 2015, pp. 178–183.
- [17] L. Lao, D. M. Manzano, H. van Someren, I. Ashraf, C. G. Almudever, Mapping of quantum circuits onto nisc superconducting processors, Quantum 2 (2019) 3.
- [18] C. Zhang, Y. Chen, Y. Jin, W. Ahn, Y. Zhang, E. Z. Zhang, A depth-aware swap insertion scheme for the qubit mapping problem, arXiv preprint arXiv:2002.07289 (2020).
- [19] K. E. Booth, M. Do, J. C. Beck, E. Rieffel, D. Venturelli, J. Frank, Comparing and integrating constraint programming and temporal planning for quantum circuit compilation, in: Twenty-Eighth International Conference on Automated Planning and Scheduling, 2018.

- [20] D. Venturelli, M. Do, E. G. Rieffel, J. Frank, Temporal planning for compilation of quantum approximate optimization circuits., in: Twenty-Sixth International Joint Conference on Artificial Intelligence, 2017, pp. 4440–4446.
- [21] S. Nishio, Y. Pan, T. Satoh, H. Amano, R. V. Meter, Extracting success from ibm’s 20-qubit machines using error-aware compilation, *ACM Journal on Emerging Technologies in Computing Systems (JETC)* 16 (3) (2020) 1–25.
- [22] P. Murali, J. M. Baker, A. Javadi-Abhari, F. T. Chong, M. Martonosi, Noise-adaptive compiler mappings for noisy intermediate-scale quantum computers, in: Proceedings of the Twenty-Fourth International Conference on Architectural Support for Programming Languages and Operating Systems, ACM, 2019, pp. 1015–1029.
- [23] J. Kusyk, S. M. Saeed, M. U. Uyar, Survey on quantum circuit compilation for noisy intermediate-scale quantum computers: Artificial intelligence to heuristics, *IEEE Transactions on Quantum Engineering* 2 (2021) 1–16. doi:10.1109/TQE.2021.3068355.
- [24] M. Y. Siraichi, V. F. d. Santos, S. Collange, F. M. Q. Pereira, Qubit allocation, in: Proceedings of the 2018 International Symposium on Code Generation and Optimization, ACM, 2018, pp. 113–125.
- [25] M. Saeedi, R. Wille, R. Drechsler, Synthesis of quantum circuits for linear nearest neighbor architectures, *Quantum Information Processing* 10 (3) (2011) 355–377.
- [26] D. Venturelli, M. Do, E. Rieffel, J. Frank, Compiling quantum circuits to realistic hardware architectures using temporal planners, *Quantum Science and Technology* 3 (2) (2018) 025004.
- [27] A. A. de Almeida, G. W. Dueck, A. C. da Silva, Finding optimal qubit permutations for IBM’s quantum computer architectures, in: Proceedings of the 32nd Symposium on Integrated Circuits and Systems Design, 2019, pp. 1–6.
- [28] R. Rasconi, A. Oddi, An innovative genetic algorithm for the quantum circuit compilation problem, in: Proceedings of the AAAI Conference on Artificial Intelligence, Vol. 33, 2019, pp. 7707–7714.
- [29] A. Oddi, R. Rasconi, Greedy randomized search for scalable compilation of quantum circuits, in: International Conference on the Integration of Constraint Programming, Artificial Intelligence, and Operations Research, Springer, 2018, pp. 446–461.
- [30] W. Finigan, M. Cubeddu, T. Lively, J. Flick, P. Narang, Qubit allocation for noisy intermediate-scale quantum computers, arXiv preprint arXiv:1810.08291 (2018).
- [31] D. Silver, A. Huang, C. J. Maddison, A. Guez, L. Sifre, G. Van Den Driessche, J. Schrittwieser, I. Antonoglou, V. Panneershelvam, M. Lanctot, et al., Mastering the game of go with deep neural networks and tree search, *Nature* 529 (7587) (2016) 484.
- [32] D. Silver, J. Schrittwieser, K. Simonyan, I. Antonoglou, A. Huang, A. Guez, T. Hubert, L. Baker, M. Lai, A. Bolton, et al., Mastering the game of go without human knowledge, *Nature* 550 (7676) (2017) 354–359.
- [33] C. B. Browne, E. Powley, D. Whitehouse, S. M. Lucas, P. I. Cowling, P. Rohlfshagen, S. Tavener, D. Perez, S. Samothrakis, S. Colton, A survey of monte carlo tree search methods, *IEEE Transactions on Computational Intelligence and AI in games* 4 (1) (2012) 1–43.
- [34] L. Kocsis, C. Szepesvári, Bandit based monte-carlo planning, in: 15th European Conference on Machine Learning, Springer, 2006, pp. 282–293.
- [35] G. M. J. Chaslot, M. H. Winands, H. J. V. D. HERIK, J. W. Uiterwijk, B. Bouzy, Progressive strategies for monte-carlo tree search, *New Mathematics and Natural Computation* 4 (03) (2008) 343–357.
- [36] X. Zhou, Y. Feng, S. Li, A monte carlo tree search framework for quantum circuit transformation, in: 2020 IEEE/ACM International Conference on Computer-Aided Design (ICCAD), IEEE, 2020, pp. 1–7.

- [37] T. Itoko, R. Raymond, T. Imamichi, A. Matsuo, A. W. Cross, Quantum circuit compilers using gate commutation rules, in: Proceedings of the 24th Asia and South Pacific Design Automation Conference, ACM, 2019, pp. 191–196.
- [38] M. Y. Siraichi, V. F. dos Santos, C. Collange, F. M. Q. Pereira, Qubit allocation as a combination of subgraph isomorphism and token swapping, Proc. ACM Program. Lang. 3 (OOPSLA) (2019) 120:1–120:29. doi:10.1145/3360546.  
URL <https://doi.org/10.1145/3360546>
- [39] B. Nash, V. Gheorghiu, M. Mosca, Quantum circuit optimizations for NISQ architectures, Quantum Science and Technology 5 (2) (2020) 025010.
- [40] C. Zhang, A. B. Hayes, L. Qiu, Y. Jin, Y. Chen, E. Z. Zhang, Time-optimal qubit mapping, in: Proceedings of the 26th ACM International Conference on Architectural Support for Programming Languages and Operating Systems, 2021, pp. 360–374.
- [41] V. Gheorghiu, S. M. Li, M. Mosca, P. Mukhopadhyay, Reducing the CNOT count for Clifford+T circuits on NISQ architectures, arXiv preprint arXiv:2011.12191 (2020).
- [42] B. Tan, J. Cong, Optimality study of existing quantum computing layout synthesis tools, IEEE Transactions on Computers (accepted).

For detailed experimental results, please refer to the appendix, where mcts-s and mcts-d denote, respectively, the algorithms MCTS-Size and MCTS-Depth; and mcts-s+r and mcts-d+r denote, respectively, the corresponding variants that uses remote CNOTs.

## A Qiskit Quantum Circuits Set Benchmarks

Table 4: Detailed results of MCTS-Size and MCTS-Size+r on IBM Q20 with naive initial mappings (Circuits are extracted from Qiskit library and each SWAP is decomposed into 3 CNOTs).

Circuit Name	#gate input	#cnot input	depth input	#gate mcts-s	depth mcts-s	#gate mcts-s+r	depth mcts-s+r
AND_10	3067	1532	2556	3199	2584	3241	2674
AND_11	6139	3068	5116	6397	5239	6331	5233
AND_12	12283	6140	10236	13000	10292	12763	10544
AND_13	24571	12284	20476	25765	20506	25411	21004
AND_14	49147	24572	40956	50998	40983	50740	41985
AND_5	105	36	81	123	84	123	94
AND_6	187	92	156	217	174	214	170
AND_7	379	188	316	433	332	421	340
AND_8	763	380	636	847	678	832	676
AND_9	1531	764	1276	1675	1302	1633	1324
excitation_preserving_10	1930	540	374	2140	898	2146	978
excitation_preserving_11	2354	660	414	2633	1303	2639	1250
excitation_preserving_12	2820	792	454	3114	1477	3117	1443
excitation_preserving_13	3328	936	494	3691	1807	3697	1762
excitation_preserving_14	3878	1092	534	4286	1973	4271	1919
excitation_preserving_15	4470	1260	574	4944	2240	5010	2359
excitation_preserving_5	440	120	174	485	285	476	265
excitation_preserving_6	654	180	214	717	423	717	423
excitation_preserving_7	910	252	254	1003	480	1003	480
excitation_preserving_8	1208	336	294	1340	694	1340	694
excitation_preserving_9	1548	432	334	1728	769	1728	756
grover_operator_10	3110	1532	2562	3242	2590	3281	2680
grover_operator_11	6186	3068	5122	6444	5245	6378	5239
grover_operator_12	12334	6140	10242	13051	10299	12754	10486
grover_operator_13	24626	12284	20482	25820	20512	25778	21168
grover_operator_14	49206	24572	40962	51057	40989	50799	41991
grover_operator_5	128	36	87	146	90	146	102
grover_operator_6	214	92	162	244	179	241	175
grover_operator_7	410	188	322	464	339	452	346
grover_operator_8	798	380	642	888	666	867	682
grover_operator_9	1570	764	1282	1714	1309	1672	1330
hidden_linear_10	68	16	21	98	45	101	45
hidden_linear_11	76	18	23	118	61	115	43
hidden_linear_12	84	20	25	123	57	126	51
hidden_linear_13	92	22	27	137	66	134	61
hidden_linear_14	100	24	29	148	64	145	57
hidden_linear_15	108	26	31	162	66	159	64
hidden_linear_5	28	6	11	43	26	40	28
hidden_linear_6	36	8	13	57	28	57	28
hidden_linear_7	44	10	15	62	36	62	36
hidden_linear_8	52	12	17	73	39	73	33
hidden_linear_9	60	14	19	87	40	90	46
inner_product_10	15	5	3	15	3	15	3
inner_product_12	18	6	3	33	17	33	17
inner_product_14	21	7	3	39	11	39	11
inner_product_6	9	3	3	21	11	21	11
inner_product_8	12	4	3	24	14	24	14
integer_comparator_10	110	42	73	134	82	134	82
integer_comparator_12	140	54	93	182	114	182	123
integer_comparator_14	170	66	113	224	136	227	160
integer_comparator_6	50	18	33	65	43	65	43
integer_comparator_8	80	30	53	95	62	95	62
IQP_10	225	78	72	294	155	294	179
IQP_11	276	98	79	363	196	363	186
IQP_12	319	114	84	415	247	418	197
IQP_13	364	130	92	469	224	481	258
IQP_14	430	156	104	547	286	562	329
IQP_15	483	176	104	642	285	648	327

Table 4: Detailed results of MCTS-Size and MCTS-Size+r on IBM Q20 with naive initial mappings (Circuits are extracted from Qiskit library and each SWAP is decomposed into 3 CNOTs).

Circuit Name	#gate input	#cnot input	depth input	#gate mcts-s	depth mcts-s	#gate mcts-s+r	depth mcts-s+r
IQP_5	60	18	32	78	48	78	48
IQP_6	88	28	40	118	77	118	77
IQP_7	116	38	48	152	88	149	87
IQP_8	163	56	56	202	112	202	112
IQP_9	191	66	60	242	143	245	120
OR_10	3086	1532	2557	3218	2585	3263	2672
OR_11	6160	3068	5117	6418	5240	6352	5234
OR_12	12306	6140	10237	13023	10293	12726	10481
OR_13	24596	12284	20477	25790	20507	25433	21008
OR_14	49174	24572	40957	51025	40984	50767	41986
OR_5	114	36	82	132	85	132	85
OR_6	198	92	157	228	175	225	171
OR_7	392	188	317	446	333	434	341
OR_8	778	380	637	862	679	847	677
OR_9	1548	764	1277	1692	1303	1650	1325
phase_estimation_10	3981	1586	2604	4071	2673	4071	2673
phase_estimation_11	7863	3138	5172	7956	5259	7956	5257
phase_estimation_12	15590	6228	10300	15701	10386	15704	10397
phase_estimation_13	31002	12392	20548	31131	20702	31125	20730
phase_estimation_5	126	48	84	153	96	153	99
phase_estimation_6	263	102	172	290	190	290	190
phase_estimation_7	525	206	340	570	372	567	369
phase_estimation_8	1032	408	668	1077	691	1074	695
phase_estimation_9	2024	804	1316	2087	1361	2090	1373
phase_oracle_10	896	380	636	986	660	944	668
phase_oracle_11	3586	1532	2556	3745	2652	3700	2624
phase_oracle_12	3586	1532	2556	3745	2652	3700	2624
phase_oracle_13	14340	6140	10236	14955	10263	14922	10555
phase_oracle_14	14340	6140	10236	14955	10263	14778	10502
phase_oracle_5	52	20	36	61	45	64	45
phase_oracle_6	52	20	36	61	45	61	45
phase_oracle_7	222	92	156	252	165	249	167
phase_oracle_8	222	92	156	252	165	249	167
phase_oracle_9	896	380	636	986	660	968	668
piecewise_chebyshev_11	9331	3520	7059	9814	7305	9844	7404
piecewise_chebyshev_13	16649	6282	12639	17447	13184	17393	13147
piecewise_chebyshev_15	27079	10218	20602	28285	21489	28432	21481
piecewise_chebyshev_5	469	178	353	499	367	499	367
piecewise_chebyshev_7	1799	678	1340	1925	1436	1925	1433
piecewise_chebyshev_9	4567	1722	3435	4921	3678	4912	3663
qft_10	250	105	74	316	162	331	160
qft_11	301	125	82	394	210	394	210
qft_12	360	150	90	465	246	462	266
qft_13	421	174	98	559	329	562	339
qft_14	490	203	106	655	346	628	359
qft_15	561	231	114	738	373	762	340
qft_5	61	26	34	79	58	79	58
qft_6	90	39	42	114	85	123	83
qft_7	121	51	50	154	98	154	98
qft_8	160	68	58	202	134	202	134
qft_9	201	84	66	264	128	264	128
quadratic_form_10	581	252	292	722	395	725	383
quadratic_form_11	684	296	334	855	479	876	490
quadratic_form_12	792	342	376	1005	580	975	594
quadratic_form_13	905	390	418	1130	637	1130	637
quadratic_form_14	1023	440	460	1266	738	1251	752
quadratic_form_15	1146	492	502	1461	817	1455	809
quadratic_form_5	141	62	82	165	109	165	109
quadratic_form_6	219	96	124	264	169	264	169
quadratic_form_7	302	132	166	362	210	362	210
quadratic_form_8	390	170	208	477	286	468	274



Table 4: Detailed results of MCTS-Size and MCTS-Size+r on IBM Q20 with naive initial mappings (Circuits are extracted from Qiskit library and each SWAP is decomposed into 3 CNOTs).

Circuit Name	#gate input	#cnot input	depth input	#gate mcts-s	depth mcts-s	#gate mcts-s+r	depth mcts-s+r
quadratic_form_9	483	210	250	606	374	615	366
quantum_volume_10	550	150	70	613	176	613	176
quantum_volume_11	605	165	77	701	248	701	248
quantum_volume_12	792	216	84	921	269	915	299
quantum_volume_13	858	234	91	990	331	993	351
quantum_volume_14	1078	294	98	1246	398	1258	441
quantum_volume_15	1155	315	105	1359	454	1356	458
quantum_volume_5	110	30	35	125	50	128	48
quantum_volume_6	198	54	42	222	77	222	77
quantum_volume_7	231	63	49	255	106	255	106
quantum_volume_8	352	96	56	388	143	388	143
quantum_volume_9	396	108	63	447	156	447	156
weighted_adder_12	863	319	571	1046	743	1046	749
weighted_adder_15	1466	538	1003	1799	1263	1808	1280
weighted_adder_6	96	38	63	114	69	114	69
weighted_adder_9	367	137	229	463	300	451	279
excitation_preserving_16	5104	1440	614	5701	2745	5758	2750
excitation_preserving_17	5780	1632	654	6605	2911	6539	2698
excitation_preserving_18	6498	1836	694	7371	3077	7329	3147
excitation_preserving_19	7258	2052	734	8134	3243	8200	3522
excitation_preserving_20	8060	2280	774	9149	3973	9179	4219
hidden_linear_16	116	28	33	176	68	170	70
hidden_linear_17	124	30	35	190	87	184	77
hidden_linear_18	132	32	37	204	84	195	73
hidden_linear_19	140	34	39	203	96	209	92
hidden_linear_20	148	36	41	223	97	220	97
inner_product_16	24	8	3	57	17	57	31
inner_product_18	27	9	3	60	21	60	21
inner_product_20	30	10	3	45	6	45	6
integer_comparator_16	200	78	133	269	173	269	173
integer_comparator_18	230	90	153	311	179	314	187
integer_comparator_20	260	102	173	347	202	350	201
IQP_16	543	198	120	717	352	711	343
IQP_17	619	228	125	835	407	853	388
IQP_18	681	252	132	909	449	924	460
IQP_19	756	280	144	1005	478	1029	482
IQP_20	830	310	148	1115	493	1136	473
piecewise_chebyshev_17	41179	15538	31375	43132	32720	43618	33075
qft_16	640	264	122	856	472	832	454
qft_17	721	296	130	964	479	952	485
qft_18	810	333	138	1104	502	1107	536
qft_19	901	369	146	1219	569	1267	638
qft_20	1000	410	154	1360	617	1375	658
quadratic_form_16	1274	546	544	1667	949	1607	949
quadratic_form_17	1407	602	586	1827	1021	1818	1026
quadratic_form_18	1545	660	628	1998	1069	1962	1040
quadratic_form_19	1688	720	670	2174	1213	2183	1229
quadratic_form_20	1836	782	712	2400	1337	2361	1362
quantum_volume_16	1408	384	112	1663	598	1663	547
quantum_volume_17	1496	408	119	1802	519	1784	529
quantum_volume_18	1782	486	126	2109	554	2118	641
quantum_volume_19	1881	513	133	2223	668	2310	606
quantum_volume_20	2200	600	140	2728	831	2701	836
weighted_adder_18	2301	843	1592	2844	1972	2715	1944
Summary	603654	260589	413734	644664	455560	642261	462746

Table 5: Detailed results of MCTS-Depth and MCTS-Depth+r on IBM Q20  
with naive initial mappings (Circuits are extracted from Qiskit library and  
each SWAP is decomposed into 3 CNOTs).

Circuit Name	#gate input	#cnot input	depth input	#gate mcts-d	depth mcts-d	#gate mcts-d+r	depth mcts-d+r
AND_10	3067	1532	2556	3289	2585	3196	2597
AND_11	6139	3068	5116	6385	5143	6298	5193
AND_12	12283	6140	10236	12727	10260	12568	10373
AND_13	24571	12284	20476	25411	20506	25135	20738
AND_14	49147	24572	40956	50740	40989	50173	41583
AND_5	105	36	81	126	86	129	86
AND_6	187	92	156	217	168	223	165
AND_7	379	188	316	439	329	454	328
AND_8	763	380	636	868	645	883	651
AND_9	1531	764	1276	2026	1291	1648	1312
excitation_preserving_10	1930	540	374	2302	732	2251	762
excitation_preserving_11	2354	660	414	2831	915	2879	967
excitation_preserving_12	2820	792	454	3441	1089	3591	1082
excitation_preserving_13	3328	936	494	3958	1227	4276	1295
excitation_preserving_14	3878	1092	534	4739	1387	4742	1500
excitation_preserving_15	4470	1260	574	5457	1671	5295	1600
excitation_preserving_5	440	120	174	512	240	521	212
excitation_preserving_6	654	180	214	750	314	747	297
excitation_preserving_7	910	252	254	1084	370	1105	407
excitation_preserving_8	1208	336	294	1487	484	1427	494
excitation_preserving_9	1548	432	334	1824	611	1941	631
grover_operator_10	3110	1532	2562	3260	2589	3239	2603
grover_operator_11	6186	3068	5122	6519	5149	6345	5199
grover_operator_12	12334	6140	10242	12778	10267	12619	10379
grover_operator_13	24626	12284	20482	26243	20501	25280	20746
grover_operator_14	49206	24572	40962	50907	40996	50643	41864
grover_operator_5	128	36	87	155	92	155	92
grover_operator_6	214	92	162	244	173	244	173
grover_operator_7	410	188	322	452	338	464	338
grover_operator_8	798	380	642	903	653	882	656
grover_operator_9	1570	764	1282	1693	1299	2245	1302
hidden_linear_10	68	16	21	122	40	113	38
hidden_linear_11	76	18	23	136	45	136	41
hidden_linear_12	84	20	25	150	46	144	44
hidden_linear_13	92	22	27	182	56	173	47
hidden_linear_14	100	24	29	217	60	166	51
hidden_linear_15	108	26	31	240	62	246	69
hidden_linear_5	28	6	11	52	19	52	19
hidden_linear_6	36	8	13	69	22	69	23
hidden_linear_7	44	10	15	74	27	80	27
hidden_linear_8	52	12	17	91	31	85	29
hidden_linear_9	60	14	19	108	36	120	34
inner_product_10	15	5	3	15	3	15	3
inner_product_12	18	6	3	33	9	36	9
inner_product_14	21	7	3	45	9	45	12
inner_product_6	9	3	3	24	8	24	8
inner_product_8	12	4	3	24	8	27	8
integer_comparator_10	110	42	73	194	78	194	88
integer_comparator_12	140	54	93	245	104	227	112
integer_comparator_14	170	66	113	233	123	293	124
integer_comparator_6	50	18	33	77	41	77	41
integer_comparator_8	80	30	53	95	57	98	57
IQP_10	225	78	72	399	132	345	112
IQP_11	276	98	79	468	152	507	155
IQP_12	319	114	84	523	177	511	156
IQP_13	364	130	92	703	192	604	186
IQP_14	430	156	104	727	217	811	241
IQP_15	483	176	104	933	240	816	247
IQP_5	60	18	32	93	39	99	39
IQP_6	88	28	40	118	51	139	52
IQP_7	116	38	48	188	67	179	69

Table 5: Detailed results of MCTS-Depth and MCTS-Depth+r on IBM Q20  
with naive initial mappings (Circuits are extracted from Qiskit library and  
each SWAP is decomposed into 3 CNOTs).

Circuit Name	#gate input	#cnot input	depth input	#gate mcts-d	depth mcts-d	#gate mcts-d+r	depth mcts-d+r
IQP_8	163	56	56	307	92	295	104
IQP_9	191	66	60	284	102	347	122
OR_10	3086	1532	2557	3449	2583	3215	2598
OR_11	6160	3068	5117	6406	5144	6319	5194
OR_12	12306	6140	10237	12750	10261	12591	10374
OR_13	24596	12284	20477	25703	20501	25070	20745
OR_14	49174	24572	40957	50767	40990	50611	41858
OR_5	114	36	82	138	87	138	87
OR_6	198	92	157	231	166	228	169
OR_7	392	188	317	449	327	446	334
OR_8	778	380	637	883	647	901	652
OR_9	1548	764	1277	1812	1293	1668	1313
phase_estimation_10	3981	1586	2604	4134	2662	4095	2642
phase_estimation_11	7863	3138	5172	7989	5226	8007	5237
phase_estimation_12	15590	6228	10300	15770	10367	15743	10374
phase_estimation_13	31002	12392	20548	31254	20653	31215	20642
phase_estimation_5	126	48	84	159	93	162	94
phase_estimation_6	263	102	172	299	189	299	189
phase_estimation_7	525	206	340	600	367	573	355
phase_estimation_8	1032	408	668	1143	697	1107	690
phase_estimation_9	2024	804	1316	2141	1357	2141	1358
phase_oracle_10	896	380	636	956	648	947	654
phase_oracle_11	3586	1532	2556	3730	2582	3700	2610
phase_oracle_12	3586	1532	2556	3739	2571	3700	2607
phase_oracle_13	14340	6140	10236	14916	10260	14676	10371
phase_oracle_14	14340	6140	10236	14916	10260	14649	10381
phase_oracle_5	52	20	36	70	39	70	39
phase_oracle_6	52	20	36	70	39	70	39
phase_oracle_7	222	92	156	255	162	255	162
phase_oracle_8	222	92	156	255	162	255	162
phase_oracle_9	896	380	636	956	648	947	654
piecewise_chebyshev_11	9331	3520	7059	9898	7202	9991	7198
piecewise_chebyshev_13	16649	6282	12639	17744	12948	17702	12921
piecewise_chebyshev_15	27079	10218	20602	28774	21092	28459	20982
piecewise_chebyshev_5	469	178	353	514	356	520	359
piecewise_chebyshev_7	1799	678	1340	1961	1371	1964	1374
piecewise_chebyshev_9	4567	1722	3435	4924	3508	4990	3513
qft_10	250	105	74	397	127	388	122
qft_11	301	125	82	481	157	574	177
qft_12	360	150	90	705	192	669	196
qft_13	421	174	98	865	229	685	216
qft_14	490	203	106	871	231	994	257
qft_15	561	231	114	897	278	1008	282
qft_5	61	26	34	109	44	112	44
qft_6	90	39	42	135	59	159	69
qft_7	121	51	50	193	77	163	76
qft_8	160	68	58	280	101	265	94
qft_9	201	84	66	366	125	297	120
quadratic_form_10	581	252	292	896	362	827	368
quadratic_form_11	684	296	334	1014	451	1050	445
quadratic_form_12	792	342	376	1251	528	1185	504
quadratic_form_13	905	390	418	1370	580	1358	551
quadratic_form_14	1023	440	460	1626	620	1578	622
quadratic_form_15	1146	492	502	1812	708	1812	720
quadratic_form_5	141	62	82	189	100	186	93
quadratic_form_6	219	96	124	348	145	297	140
quadratic_form_7	302	132	166	404	200	404	193
quadratic_form_8	390	170	208	543	253	531	250
quadratic_form_9	483	210	250	741	313	840	331
quantum_volume_10	550	150	70	703	165	748	181
quantum_volume_11	605	165	77	815	206	815	209

Table 5: Detailed results of MCTS-Depth and MCTS-Depth+r on IBM Q20  
with naive initial mappings (Circuits are extracted from Qiskit library and  
each SWAP is decomposed into 3 CNOTs).

Circuit Name	#gate input	#cnot input	depth input	#gate mcts-d	depth mcts-d	#gate mcts-d+r	depth mcts-d+r
quantum_volume_12	792	216	84	1074	248	1140	272
quantum_volume_13	858	234	91	1173	285	1170	285
quantum_volume_14	1078	294	98	1447	343	1492	370
quantum_volume_15	1155	315	105	1575	356	1611	391
quantum_volume_5	110	30	35	155	50	152	50
quantum_volume_6	198	54	42	240	74	303	81
quantum_volume_7	231	63	49	282	104	288	79
quantum_volume_8	352	96	56	433	111	478	158
quantum_volume_9	396	108	63	480	124	489	156
weighted_adder_12	863	319	571	1247	646	1175	619
weighted_adder_15	1466	538	1003	2072	1129	2093	1121
weighted_adder_6	96	38	63	114	69	114	69
weighted_adder_9	367	137	229	529	263	526	254
excitation_preserving_16	5104	1440	614	6376	1849	6433	1933
excitation_preserving_17	5780	1632	654	7034	2089	7316	2121
excitation_preserving_18	6498	1836	694	8295	2423	8037	2360
excitation_preserving_19	7258	2052	734	9361	2738	9118	2548
excitation_preserving_20	8060	2280	774	10235	2747	10619	2968
hidden_linear_16	116	28	33	236	68	218	64
hidden_linear_17	124	30	35	259	69	244	70
hidden_linear_18	132	32	37	243	78	222	69
hidden_linear_19	140	34	39	263	76	257	81
hidden_linear_20	148	36	41	322	86	286	83
inner_product_16	24	8	3	72	14	84	14
inner_product_18	27	9	3	105	17	90	17
inner_product_20	30	10	3	60	12	54	10
integer_comparator_16	200	78	133	383	154	344	155
integer_comparator_18	230	90	153	386	159	422	165
integer_comparator_20	260	102	173	473	195	416	187
IQP_16	543	198	120	957	289	996	296
IQP_17	619	228	125	1135	319	1144	315
IQP_18	681	252	132	1365	345	1284	339
IQP_19	756	280	144	1362	374	1347	381
IQP_20	830	310	148	1409	389	1451	374
piecewise_chebyshev_17	41179	15538	31375	43504	32032	43387	32055
qft_16	640	264	122	1108	330	1141	334
qft_17	721	296	130	1297	373	1348	382
qft_18	810	333	138	1416	407	1632	441
qft_19	901	369	146	1582	439	1534	420
qft_20	1000	410	154	1828	478	1816	485
quadratic_form_16	1274	546	544	1928	791	2120	771
quadratic_form_17	1407	602	586	2385	873	2199	825
quadratic_form_18	1545	660	628	2550	953	2487	941
quadratic_form_19	1688	720	670	2846	1045	2756	1012
quadratic_form_20	1836	782	712	3141	1132	3015	1105
quantum_volume_16	1408	384	112	1951	472	1927	460
quantum_volume_17	1496	408	119	2114	489	2249	542
quantum_volume_18	1782	486	126	2601	583	2499	547
quantum_volume_19	1881	513	133	2721	586	2691	541
quantum_volume_20	2200	600	140	3424	749	3394	755
weighted_adder_18	2301	843	1592	3396	1794	3339	1780
Summary	603654	260589	413734	668646	440971	663987	445034